This is a repository copy of *Quantitative analysis of the sedimentary architecture of eolian successions developed under icehouse and greenhouse climatic conditions*.

White Rose Research Online URL for this paper:
https://eprints.whiterose.ac.uk/170702/

Version: Accepted Version

1 Title of manuscript: Quantitative analysis of the sedimentary

2 architecture of eolian successions developed under icehouse and

3 greenhouse climatic conditions

4 **Grace I.E. Cosgrove[1], Luca Colombera[1], Nigel P. Mountney[1]**

5 *[1] Fluvial & Eolian Research Group, School of Earth and Environment, University of Leeds,*

6 *Leeds, LS2 9JT, UK*

7 **ABSTRACT**

8 The continental terrestrial record preserves an archive of how ancient sedimentary systems

9 respond to and record changes in global climate. A database-driven quantitative assessment

10 reveals differences in the preserved sedimentary architectures of siliciclastic eolian systems

11 with broad geographic and stratigraphic distribution, developed under icehouse versus

12 greenhouse climatic conditions. Over 5,600 geological entities, including architectural

13 elements, facies, sediment textures and bounding surfaces, have been analyzed from 34

14 eolian systems of Paleoproterozoic to Cenozoic ages. Statistical analyses have been

15 performed on the abundance, composition, preserved thickness, and arrangement of different

16 eolian lithofacies, architectural elements and bounding surfaces. Results demonstrate that

17 preserved sedimentary architectures of icehouse and greenhouse systems differ markedly.

18 Eolian dune, sandsheet and interdune architectural elements that accumulated under icehouse

19 conditions are significantly thinner relative to their greenhouse counterparts; this is observed

20 across all basin settings, supercontinents, geological ages, and dune-field physiographic

21 settings. However, this difference between icehouse and greenhouse eolian systems is

22 exclusively observed for paleolatitudes <30°, suggesting that climate-induced changes in the

23 strength and circulation patterns of trade winds may have partly controlled eolian sand

accumulation. These changes acted in combination with variations in water-table levels, sand supply and sand transport, ultimately influencing the nature of long-term sediment preservation. During icehouse episodes, Milankovitch-cyclicity resulted in deposits typified by glacial accumulation and interglacial deflation. Greenhouse conditions promoted the accumulation of eolian elements into the geological record due to elevated water tables and biogenic and chemical stabilizing agents, which could protect deposits from wind-driven deflation. In the context of a rapidly changing climate, the results presented here can help predict the impact of climate change on Earth surface processes.

Keywords: Eolian, Database, Icehouse, Greenhouse, Climate

INTRODUCTION

The current rate of release of carbon dioxide into the atmosphere, largely through the anthropogenic combustion of fossil fuels, is occurring at a geologically unprecedented rate (Kidder and Worsley, 2011; Andrew, 2020; Peters et al., 2020). The associated changes in global climate, and the impact of such climate change in terms of its influence on Earth surface processes, has significant scientific and societal implications (e.g., IPCC, 2007 and references therein). Quantifying the response of Earth's geosphere to changes in climate therefore represents one of the foremost issues faced in modern sedimentology (Hodgson et al., 2018). Given the paucity of long-term (> 100 years) instrumental records, analysis of the sedimentary record is critical for understanding the impact of climate change on Earth surface processes. The continental terrestrial record preserves an archive of how ancient sedimentary systems respond to, and record, changes in global climate, over time scales far beyond the range of human experience. Observational evidence from the ancient sedimentary record therefore provides a means to both quantify past responses and predict future responses of the Earth's surface processes to shifts in global climate.

48   Throughout geological history, the Earth's climate can be subdivided into periods

49   characterized by the presence or absence of major continental ice-sheets and polar ice (Fig. 1)

50   – two climate states referred to as icehouse and greenhouse, respectively (Frakes et al., 1992;

51   Price et al., 1998; Cromwell, 1999). The preserved eolian sedimentary record, which spans

52   over three billion years of Earth history from the Archean to the present day (Clemmensen,

53   1985; Dott et al., 1986; Voss, 2002; Cather et al., 2008; Simpson et al., 2012; Rodríguez-

54   López et al., 2014) is a valuable archive of the continental landscape response to periodic

55   fluctuations between icehouse and greenhouse worlds.

56   A comprehensive global-scale quantitative comparison of the preserved architectures of sand-

57   dominated eolian sedimentary systems (ergs, *sensu* Wilson, 1973) accumulated and preserved

58   under icehouse and greenhouse conditions has not been undertaken previously. Prior research

59   on this topic has been primarily reported in the form of largely qualitative accounts,

60   commonly for individual case studies or regions from eolian successions associated with

61   either greenhouse (e.g., Crabaugh and Kocurek, 1993; Kocurek et al., 1992; Jones and

62   Blakey, 1997; Benan and Kocurek, 2000; Kocurek and Day, 2018) or icehouse (e.g., Cowan,

63   1993; Meadows and Beach, 1993; Clemmensen and Abrahamsen, 1983) climatic conditions.

64   In addition to the effects of climate, eolian sedimentary systems are sensitive to a variety of

65   additional forcings, including rate and type of sediment supply, sea level, tectonic

66   configuration, basin setting and dune-field physiographic setting (e.g., Blakey and Middleton,

67   1983; Blakey, 1988; Mountney et al., 1999; Kocurek et al., 2001; Nichols, 2005; Soria et al.,

68   2011). As such, isolating and quantifying the global effects of climate as a control on

69   sedimentary systems is difficult, especially for individual case studies. To address this

70   problem, this study uses a global dataset derived from 42 published articles associated with

71   34 ancient eolian successions (Fig. 1).

72 The aim of this study is to quantify relationships between global climate states and preserved

73 eolian sedimentary architecture at multiple scales of observation. This study addresses three

74 main research questions: (i) How are the characters of preserved eolian and related

75 architectural elements, and their bounding surfaces affected by fluctuations in global climate

76 states? (ii) Does the prevailing global climate influence the sedimentology and stratigraphic

77 architecture of preserved eolian sedimentary successions? (iii) Can the effects of icehouse

78 and greenhouse conditions on preserved eolian sedimentary architectures be isolated from

79 those of supercontinental setting, paleolatitude, basin setting and dune-field physiographic

80 setting?

81 **Background: an Overview of the Icehouse and Greenhouse Earth**

82 Icehouse and greenhouse conditions account for approximately 15% and 85% of Earth

83 history, respectively (Fig. 1; Frakes et al., 1992; Crowell, 1999; Link, 2009). Global shifts

84 between icehouse and greenhouse conditions are caused by the cumulative effects of

85 astronomical, biogeochemical and tectonic events, which interact with each other and lead to

86 the development of feedback mechanisms that act to influence global climate. Icehouse and

87 greenhouse conditions are respectively defined by the presence or absence of major polar ice-

88 sheets that calve marine icebergs (Kidder and Worsley, 2012). Greenhouse conditions can,

89 however, be associated with seasonal sea ice, alpine glaciers and transient polar ice-caps

90 (Frakes, 1992; Kidder and Worsley, 2012).

91 Five major icehouse periods are recognized in Earth history (Fig. 1): the Huronian (2400-

92 2100 Ma; Coleman, 1907; Evans et al., 1997), the Cryogenian (720-635 Ma; Knoll and

93 Walter, 1992; Bowring et al., 2003; Hoffman et al., 2004), the Late Ordovician and Early

94 Silurian glaciations, also known as the Andean-Saharan (450-420 Ma; Brenchley et al.,

95 1994), the Late Paleozoic (360-260 Ma; Montanez and Poulsen, 2013; Goddéris et al., 2017),

96 and the current Cenozoic icehouse conditions that persist today (since 33.9 Ma; Frakes et al.,

97   1992). The five major icehouse intervals have each lasted for tens of millions of years and are

98   each associated with mid-latitude glaciation down to sea level (Frakes et al., 1992; Cromwell,

99   1999). Relative to greenhouse conditions, icehouse conditions are typically associated with:

100 (i) lower atmospheric levels of carbon dioxide; (ii) lower sea levels and sea-surface

101 temperatures; (iii) strong thermohaline deep-ocean circulation; (iv) strong marine polar-to-

102 equatorial thermal contrasts; (v) increased wind velocities at low-latitudes (< 30º) leading to

103 higher wind shear and higher wind-related erosive power (Fig 2; Frakes et al., 1992;

104 Cromwell, 1999; Forster et al., 2007; Kidder and Worsley, 2010, 2012).

105 Within long-lived icehouse periods, climatic conditions are known to fluctuate between

106 glacial and interglacial episodes, which give rise to the waxing and waning of continental

107 glaciations; these cycles of glacial expansion and retreat are superimposed onto overall

108 longer-term net icehouse conditions. In the most recent Cenozoic icehouse, glacial and

109 interglacial cycles occur at quasi-100 kyr intervals, with shorter 41 kyr and 21 kyr quasi-

110 cycles superimposed (Shackleton et al., 1999). The cyclic regularity of glacial and

111 interglacial periods is attributed dominantly to variations in the Earth's orbital parameters –

112 the so-called Milankovitch cyclicity. The effects on the sedimentation of glacial and

113 interglacial oscillations are well documented in the deep-sea sedimentary record (e.g., Rea

114 and Janeck, 1981; Hovan et al., 1991; Petit et al., 1991; Winckler et al., 2008). For example,

115 eolian dust supply to the deep sea is greater under glacial conditions, relative to interglacial

116 conditions (e.g., Woodard et al., 2011), as a consequence of heightened aridity and stronger

117 wind strengths during glacial episodes.

118 **METHODOLOGY**

119 **Case Studies and Associated Metrics**

120   Thirty-four case studies, each representing an ancient eolian sedimentary succession (Fig. 1,

121   Table 1), and associated with detailed datasets from 42 published articles, have been analyzed

122   using the Database of Aeolian Sedimentary Architecture (DASA). DASA is a relational

123   database that stores data on a variety of eolian and associated non-eolian entities relating to

124   different scales, including architectural elements, lithofacies and bounding surfaces. DASA

125   records both qualitative and quantitative attributes that characterize the type, geometry,

126   spatial relations, hierarchical relations, temporal significance, and textural and petrophysical

127   properties of eolian and related depositional units and their bounding surfaces. In this study,

128   architectural elements, facies elements, textural properties and eolian bounding-surface types

129   documented from the selected case-study examples are analyzed.

130   For this investigation, of the 42 scientific articles considered, 24 provide accounts of systems

131   developed under icehouse conditions and 18 of greenhouse systems. Of the 34 case studies,

132   20 represent icehouse conditions and 14 represent greenhouse conditions. In total, 5,598

133   geological entities representing architectural and facies elements, textural observations and

134   eolian bounding surfaces have been analyzed: 2,772 relate to sedimentary successions

135   interpreted as having accumulated under the influence of icehouse climatic conditions; 2,826

136   under greenhouse conditions. Observations can be further categorized as follows: (i) 2,578

137   eolian and associated non-eolian architectural elements have been analyzed, of which 1,156

138   and 1,422 architectural elements relate to icehouse and greenhouse case-study systems,

139   respectively; (ii) 985 eolian facies units have been analyzed, of which 630 and 355 facies

140   relate to icehouse and greenhouse case-study systems, respectively; (iii) 1,308 textural

141   observations have been analyzed, of which 749 and 559 relate to icehouse and greenhouse

142   case-study systems, respectively; (iv) 727 bounding surfaces have been analyzed, of which

143   237 and 490 relate to icehouse and greenhouse systems, respectively.

144   Each examined case study has associated metadata describing its geological background and

145   the boundary conditions present at the time of deposition; these metadata include the

146   prevailing climate, basin setting, geologic age and paleosupercontinental setting. Metadata

147   are derived from the original source work and additional published literature.

148   Architectural elements are defined as distinct sedimentary bodies with characteristic

149   sedimentological properties (e.g., internal composition, geometry), and are the products of

150   deposition in a specific sub-environment (e.g., a dune, a wet interdune, or a fluvial channel;

151   for definitions see Table 2). Facies elements are defined as sedimentary bodies differentiated

152   on the basis of sediment composition, texture, structure, bedding geometry, fossil content, or

153   by the nature of their bounding surfaces (cf. Colombera et al., 2012, 2016).

154   At the scale of architectural and facies elements, each element is assigned an interpretation

155   derived from the original source work (e.g., a dune set at the architectural-element scale, or

156   adhesion strata at the facies-element scale). For each architectural and facies element,

157   geometric properties (element thickness, length and width) are also recorded. However, in

158   this investigation, the only geometric parameter considered in detail is the thickness of the

159   deposit.

160   The textural properties considered here are grain size, sorting and roundness. For all textural

161   properties, if a numerical value is not assigned in the original source work, but a descriptive

162   term is provided (e.g., fine-grained sand), classes are converted into numerical values

163   according to the schemes of Folk and Ward (1957) for grain size and sorting, and to the

164   Krumbein scale of roundness (Krumbein, 1941).

165   The following types of qualitative data regarding super-bounding surfaces (supersurfaces) are

166   considered here: (i) a classification of surface type (i.e., environmental significance)

167   according to the schemes of Fryberger (1993) and Kocurek (1996); (ii) the association of

168 features (sedimentary structures) indicative of substrate conditions (e.g., dry, damp, wet) and

169 associated with the state of the surface; and (iii) the occurrence of features indicative of

170 surface stabilization (e.g., Ahlbrandt et al., 1978; Loope, 1988; Basilici et al., 2009, 2020;

171 Dal' Bo et al., 2010; Krapovickas et al., 2016).

172 **Dating Ancient Eolian Successions**

173 Ancient eolian successions can be difficult to date in absolute terms due to a general paucity

174 of features suitable for numerical age-dating (Rodríguez-López et al., 2014). As such,

175 determining the time when an eolian succession accumulated can be challenging. Some

176 eolian deposits closely associated with (i) extrusive volcanics, (ii) fossil-rich marine

177 interbeds, or (iii) abundant micro-fossils present in the eolian deposits themselves, can be

178 dated and assigned a geochronometric or biostratigraphic age. More commonly, however,

179 only a relative age can be established, such that eolian successions might be interpreted in

180 terms of sequence-stratigraphic or climate-stratigraphic contexts (e.g., Mountney and Howell,

181 2000; Atchley and Loope, 1993; Jordan and Mountney, 2010, 2012). Many eolian

182 successions contain surfaces that are thought to represent and record multiple long-lived

183 depositional hiatuses in accumulation, associated with the formation of supersurfaces (e.g.,

184 Loope, 1985). For many eolian systems, the amount of time represented by such

185 supersurfaces is likely significantly greater than that represented by the eolian accumulations

186 themselves; eolian successions may be representative of only a small amount of the total

187 geological time over which the eolian system was active (Loope, 1985; cf. Ager, 1993;

188 Sadler, 1981). The preserved sedimentary record of eolian systems is highly fragmentary and

189 age ranges of eolian deposits reported in the literature may be over- or under-estimates;

190 accurately determining the ages of ancient eolian successions represents therefore an

191 unavoidable caveat.

192 For this analysis, examined case studies have been assigned to a binary 'icehouse' or

193 'greenhouse' classification scheme. Despite the above-discussed limitations on dating eolian

194 successions, given that major icehouse and greenhouse episodes span (many) tens of millions

195 of years, placing eolian successions within in an 'icehouse' or 'greenhouse' category can be

196 achieved with confidence; this study requires only that the age-range of each eolian

197 succession considered in the analysis generally falls within episodes classed as icehouse or

198 greenhouse climate states (Frakes et al., 1992; Crowell, 1999; Link, 2009). As such, precise

199 absolute ages for eolian successions considered in this analysis are not crucial.

200 Determining the age-ranges of Precambrian eolian successions can, however, be more

201 challenging, since their ages are typically more difficult to constrain (e.g., Pulvertaft, 1985;

202 Simpson et al., 2012) and they cannot necessarily be reliably assigned to an 'icehouse' or

203 'greenhouse' climate category. Only Precambrian eolian successions with age-ranges that fall

204 into to an 'icehouse' or 'greenhouse' category have been included in the analysis. In the

205 analysis and discussion all Precambrian icehouse examples are compared against all

206 Precambrian greenhouse examples.

207 There also exist eolian successions that record evidence of system development in a

208 transitional state between icehouse and greenhouse worlds (see Eriksson et al., 2019). Such

209 examples cannot readily be assigned to the binary icehouse-greenhouse classification scheme

210 used in this study. Given that the focus of this study on the eolian sedimentary signature of

211 climate extremes, examples of these "transitional" eolian successions have not been included

212 in this investigation.

213 **Carbonate Eolian Systems**

214 In this investigation, siliciclastic-dominated eolian successions have been studied; carbonate-

215 dominated eolian successions are not considered. Carbonate-dominated eolian successions

216 (eolianites) most commonly develop along humid, mid-high latitude coasts, and along arid to

217 semi-arid, mid-low latitude coasts that neighbor carbonate platforms (Clemmensen et al.,

218 1997; Brooke, 2001; Nielsen et al., 2004; Simpson et al., 2004; Frébourg et al., 2008; Fornós

219 et al., 2009; Andreucci et al., 2010). Carbonate-dominated eolian successions commonly

220 undergo early post-depositional modification, notably via the precipitation of early diagenetic

221 calcitic cements, which can readily stabilize original dune topography (Pye, 1983; Simpson et

222 al., 2004; Guern and Davaud, 2005). As such, processes of deflation, construction,

223 accumulation and preservation in carbonate eolian systems are markedly different to those of

224 most siliciclastic eolian systems. In particular, dune deflation can be retarded, and dune

225 stabilization and accumulation can be enhanced by early diagenetic cementation.

226 Mechanisms of preservation of carbonate-dominated eolian deposits in relation to prevailing

227 climatic and sediment supply conditions differ considerably from those of siliciclastic-

228 dominated systems (Rodríguez- López et al., 2014). For these reasons, this study only

229 considers siliciclastic-dominated eolian systems and their deposits.

230 **Statistical Analysis**

231 Quantitative data, including element thickness, grain size, sorting and grain roundness have

232 been subject to statistical analysis. One-tail t-tests have been undertaken to determine if a

233 significant difference exists between the means of icehouse and greenhouse groups. To test

234 for statistical significance of differences among multiple groups (i.e. for the example

235 considering multiple supercontinents under greenhouse conditions), analysis of variance

236 (ANOVA) is applied. Post-hoc tests, using a Bonferroni correction, are applied to t-tests and

237 ANOVA tests alike. An α value of 0.05 is considered for all statistical analyses; a family-

238 wise alpha is considered when applying the Bonferroni correction.

239 **RESULTS**

240   Table 3 provides a summary of results of statistical analyses discussed in the text; this

241   includes mean, median, standard deviation, and number of observations for variables of

242   interest (eolian and related element thicknesses, grain size, sorting and roundness), and the

243   results of statistical tests. In the text, for brevity only mean values are reported.

244   **Eolian Elements**

245   Differences in the characteristics of eolian and associated non-eolian architectural elements

246   are considered first (Table 2). The relative proportion of types of eolian and non-eolian

247   architectural elements is determined based on total element counts: eolian architectural

248   elements form 63% and 62% of architectural elements in the studied successions accumulated

249   under icehouse and greenhouse conditions, respectively (Fig. 3A). For all architectural

250   elements classified as 'eolian' (Table 2), statistically significant differences in element

251   thickness are found; icehouse eolian architectural elements are significantly thinner than

252   greenhouse eolian elements, with mean values of element thickness of 2.36 m and 5.47 m,

253   respectively (Fig. 4A; Table 3).

254   Of the total recorded eolian architectural elements, the percentages of elements classified as

255   'dune set', 'sandsheet' and 'interdune' are considered further (Fig. 3B; for definitions see

256   Table 2). Dune sets form 62% and 82% of all recorded observations for icehouse and

257   greenhouse eolian successions, respectively (Fig. 3B). Sandsheets form 20% and 12% of

258   icehouse and greenhouse eolian successions, respectively (Fig. 3B). Interdunes form 18% and

259   4% of the icehouse and greenhouse successions, respectively (Fig. 3B). All three major eolian

260   architectural element types (dune sets, sandsheets and interdunes) show statistically

261   significant differences in mean element thickness (Fig. 4B-D; Table 3). Under icehouse

262   conditions, dune sets, sandsheets and interdunes have mean thicknesses of 3.67 m, 0.55 m

263   and 0.88 m, respectively (Table 3). Under greenhouse conditions, dune sets, sandsheets and

264 interdunes have mean thicknesses of 5.93 m, 4.15 m and 2.00 m, respectively (Fig. 4B-D;

265 Table 3).

266 Interdune elements are considered further and subdivided into 'wet', 'damp', and 'dry' types

267 (*sensu* Kocurek, 1981) (Fig. 5A; for definitions see Table 2). In successions developed under

268 icehouse conditions, 15% of interdune elements are of wet type, 48% are of damp type, and

269 37% are of dry type. In greenhouse successions, 60% of interdune elements are of wet type,

270 30% are of damp type, and 10 % are of dry type (Fig. 5A).

271 **Non-Eolian Architectural Elements**

272 The percentage of recorded non-eolian architectural elements reported for the studied

273 successions is similar across icehouse and greenhouse successions, forming 37% and 38% of

274 recorded observations, respectively (Fig. 3C). Under both icehouse and greenhouse

275 conditions, alluvial and fluvial deposits are the most common non-eolian element types.

276 Greenhouse successions are associated with a greater percentage of sabkha elements (14% vs

277 1%). Across icehouse and greenhouse successions, there is no statistically significant

278 difference in the mean thickness of non-eolian architectural elements of any type (Table 3).

279 **Eolian Facies Elements**

280 In greenhouse successions, interdune elements of any type are most likely composed of

281 adhesion strata (92%) and plane-bed lamination (8%) (Fig. 5B). In icehouse successions, a

282 greater variety of facies-element types are recorded, including adhesion strata (38%),

283 subaqueous ripples (27%), plane-bed lamination (19%), wind-ripple lamination (14%) and

284 deflation-lag strata (2%). Icehouse sandsheet elements are dominated by adhesion strata

285 (30%), deflation-lag strata (28%) and wind-ripple strata (27%), whereas greenhouse

286 sandsheet elements mostly comprise wind-ripple strata (61%) and interfingered strata (30%)

287 (Fig. 5C; interfingered strata comprise intercalated deposits of wind-ripple, grainflow,

288 grainfall and/or plane-bed strata in varying proportions – Table 2). In icehouse successions,

289 facies elements of any type are significantly thinner than those in greenhouse successions

290 (mean thickness of 2.20 m vs 7.53 m; Fig. 4E; Table 3). For descriptions of facies units see

291 Table 2.

292 **Eolian Texture**

293 The textural properties of all eolian architectural and facies elements are now considered.

294 Systems developed under icehouse and greenhouse conditions have mean values of modal

295 grain size of 0.34 mm and 0.36 mm (both medium sand; Fig. 6A); the difference between

296 these values is not statistically significant (Table 3). Icehouse systems are characterized by a

297 higher median value of modal grain size of 0.38 mm (medium sand), relative to 0.25 mm

298 (fine-to-medium sand) for greenhouse systems (Fig. 6A).

299 In both icehouse and greenhouse systems, eolian sands are, on average, moderately well

300 sorted (icehouse = 0.57 σ, greenhouse = 0.58 σ; Fig. 6B); there is no statistically significant

301 difference between mean values of sorting (Table 3). There is, however, a statistically

302 significant difference in mean values of grain roundness between icehouse (mean = 0.57 K:

303 rounded) and greenhouse (mean = 0.77 K: well-rounded) eolian sands (Fig. 6C) (Table 3).

304 Thus, greenhouse conditions are associated with increased sand-grain textural maturity

305 relative to icehouse conditions.

306 **Eolian Surfaces**

307 Eolian supersurfaces are recorded from 12 systems; 6 each represent icehouse and

308 greenhouse conditions.

309 *Supersurface Spacing*

310 The average supersurface spacing is calculated by measuring the vertical distance between

311 two successive supersurfaces. Under icehouse conditions the mean spacing is 16.34 m

312   (standard deviation = 12.70 m; Table 3); under greenhouse conditions the mean spacing in

313   9.07 m (standard deviation = 6.34 m; Table 3). This indicates that supersurfaces are more

314   widely spaced under icehouse conditions relative to greenhouse conditions; however,

315   icehouse supersurfaces exhibit greater variability in supersurface spacing.

316   *Supersurface Descriptions*

317   Supersurfaces present in icehouse successions are classified dominantly as deflationary

318   (88%) and subordinately as bypass surfaces (12%) (Fig. 7A). In greenhouse systems,

319   deflationary and bypass supersurfaces form 67% and 33% of recorded supersurfaces,

320   respectively (Fig. 7A). The nature of the substrate associated with the supersurfaces also

321   varies considerably between icehouse and greenhouse examples. Icehouse supersurfaces are

322   dominantly associated with features indicative of a wet surface (86%) and only rarely of a

323   damp (6%) or dry (8%) surface. By contrast, in greenhouse successions, dry, damp and wet

324   surface types are associated with 12%, 24% and 64% of recorded supersurfaces, respectively

325   (Fig. 7B). When the nature of stabilization of supersurfaces is considered, 62% of icehouse

326   supersurfaces are classified as unstabilized and 38% as stabilized; for greenhouse conditions,

327   unstabilized and stabilized supersurfaces comprise 85% and 15% of recorded supersurfaces,

328   respectively (Fig. 7C).

329   **Non-Climatic Controls**

330   In addition to climate, other controls might influence the preserved style and geometry of

331   sedimentary architectures in eolian systems (e.g., Blakey and Middleton, 1983; Blakey, 1988;

332   Mountney et al., 1999; Kocurek et al., 2001; Nichols, 2005; Soria et al., 2011). To better

333   discriminate the influence of icehouse and greenhouse conditions, these other factors must be

334   considered. To this end, where data are available, comparisons between icehouse and

335   greenhouse conditions are made for: (i) specific paleogeographical configurations and

336   geological age, (ii) basin setting, (iii) paleolatitude, and (iv) dune-field (erg) physiographic

337   setting. In the following analyses, the thicknesses of eolian architectural elements (cross-

338   strata packages, dune sets, dune cosets, dune compound sets, sandsheets and interdunes) are

339   considered.

340   *Paleogeography and Geological Age*

341   Two supercontinental paleogeographic configurations spanned both icehouse and greenhouse

342   times: those associated with Precambrian supercontinents (Rodinia and Columbia), and

343   Pangea; the number of case studies falling into these categories are 6 and 11, respectively.

344   When evaluated separately for the Precambrian and Pangean supercontinental settings,

345   statistically significant differences between the mean thickness of eolian architectural

346   elements deposited under icehouse and greenhouse conditions are seen (Table 3). The mean

347   thickness of Precambrian architectural elements is 1.43 m and 5.03 m for icehouse and

348   greenhouse successions, respectively (Fig. 8A), whereas the mean thickness of Pangean

349   architectural elements is 3.41 m and 6.85 m for icehouse and greenhouse conditions,

350   respectively (Fig. 8A; Table 3).

351   *Basin Setting*

352   Of the case-study examples examined in this study, eolian systems deposited under icehouse

353   and greenhouse conditions are both recognized in the infill of sedimentary basins classified as

354   intracratonic (sag) basins, continental rifts, and foreland basins (for definitions see Table 2);

355   the number of case studies falling into these categories are 17, 4, and 3, respectively. For each

356   of these basin types, there exists a statistically significant difference between the mean values

357   of the thicknesses of eolian architectural elements deposited under icehouse and greenhouse

358   conditions (Table 3). Architectural elements accumulated under icehouse conditions in

359   intracratonic, rift and foreland basins yield mean thickness values of 1.73 m, 0.70 m and 2.11

360   m, respectively (Fig. 8B). Greenhouse architectural elements in intracratonic, rift and

361   foreland basins instead return mean thickness values of 7.63 m, 2.48 m and 4.23 m,

362   respectively (Fig. 8B; Table 3).

363   *Paleolatitude*

364   Paleolatitudes of eolian systems in this study are subdivided into the following categories: 0-

365   15°, 16-30°, 31-45°, and 46-60°; the number of case studies falling into these categories are

366   11, 12, 5, and 4, respectively. A statistically significant difference is seen between icehouse

367   and greenhouse eolian architectural element thicknesses for both paleolatitude ranges of 0-

368   15° and 16-30° (Table 3). The mean thickness of eolian architectural elements deposited in

369   paleolatitudes of 0-15° are 2.60 m and 6.38 m for icehouse and greenhouse systems,

370   respectively (Fig. 8C, 9). The mean thickness of eolian architectural elements deposited in

371   paleolatitudes of 16-30° are 2.72 m and 6.40 m for icehouse and greenhouse systems,

372   respectively (Fig. 8C, 9). However, for systems from paleolatitudes >30°, no statistically

373   significant difference is seen in mean eolian architectural element thickness (Table 3).

374   *Dune-Field (Erg) Physiographic Setting*

375   Major sand seas (ergs) can be subdivided into three generalized environmental sub-

376   components: back-, central- and fore-erg (*sensu* Porter, 1986); the number of case studies

377   falling into these categories are 8, 10, and 4, respectively. When these three dune-field

378   settings are separately analyzed, a statistically significant difference in mean eolian

379   architectural element thickness is observed in each erg-setting between icehouse and

380   greenhouse conditions (Table 3). Back-erg settings record mean eolian architectural element

381   thicknesses of 1.65 m and 2.92 m for icehouse and greenhouse conditions, respectively (Fig.

382   8D). Central-erg settings record mean eolian architectural element thicknesses of 3.39 and

383   12.83 m for icehouse and greenhouse conditions, respectively (Fig. 8D). Fore-erg settings

384   record mean eolian architectural element thicknesses of 1.87 m and 6.36 m for icehouse and

385   greenhouse conditions, respectively (Fig. 8D).

386   **DISCUSSION**

387   Prevailing climatic conditions influence the caliber of sediment and the rate of its supply,

388   sediment availability for eolian transport, water-table fluctuations, and wind regimes

389   (variability and strength), all of which themselves control resultant eolian sedimentary

390   architecture (Kocurek, 1998; Clarke and Rendell, 1998; Mountney et al., 1999; Nichols,

391   2005). The observed differences in preserved eolian-element thickness are interpreted to arise

392   from the prevailing climatic conditions associated with icehouse and greenhouse worlds. The

393   relative thicknesses of eolian successions are also dependent on the availability of

394   accommodation, and the rate at which it is created whilst a system is active. Different basin-

395   types are associated with variable rates of accommodation generation (Gregory, 1894;

396   Rosendahl, 1987; Middleton, 1989; Schlische, 1993; Einsele, 2013); the effects of basin type

397   and accommodation is discussed in section '***Basin Configuration***' below.

398   **Icehouse Conditions**

399   When dune sets, sandsheets and interdunes are considered, all are significantly thinner in

400   successions accumulated under icehouse conditions, relative to those relating to greenhouse

401   conditions. Icehouse conditions are associated with orbitally controlled oscillations

402   (Milankovitch cycles: Milankovitch, 1941; Wanless and Shepard, 1936; Dickinson et al.,

403   1994) between drier and windier glacials, favoring eolian-dune construction (Loope, 1985;

404   Mountney, 2006) – and more humid interglacials, favoring dune deflation (Rea and Janeck,

405   1981; Hovan et al., 1991; Petit et al., 1991; Kocurek, 1999; Kocurek and Lancaster, 1999;

406   Winckler et al., 2008; Woodard et al., 2011). The observation of consistently thinner eolian

407   deposits in the icehouse stratigraphic record, relative to their greenhouse counterparts, is

408   attributed to the interactions between these constructive and destructive phases, which

409   operate on timescales of ca. 100-400 kyr (Wanless and Shepard, 1936; Loope, 1985;

410   Dickinson et al., 1994).

411   *A Sequence of Eolian Accumulation and Deflation*

412   Eolian accumulation and deflation during icehouse times can be described as follows.

413   Globally, shifts from interglacial to glacial periods tend to be associated with the

414   establishment of more arid conditions, an increase in wind speeds at trade-wind latitudes, and

415   a relative fall in the level of regional water tables (Figs. 2, 10A; Rea and Janeck, 1981; Hovan

416   et al., 1991; Petit et al., 1991; Winckler et al., 2008; Woodard et al., 2011). During the initial

417   phase of glacial waxing and associated marine regression (i.e. equivalent to a falling-stage

418   systems tract; Plint and Nummedal, 2000), large volumes of sediment are made available for

419   potential eolian transport due to the exposure of areas of the continental shelf, and due to

420   water-table falls that favor the eolian remobilization of continental deposits (Loope, 1985;

421   Kocurek et al., 2001). The combination of an increase in the availability of sediment for

422   eolian transport and an increase in the potential sand-carrying capacity of the wind brought

423   about by increased wind velocity promotes an initial phase of eolian system construction and

424   accumulation (Kocurek, 1999; Kocurek and Lancaster, 1999). At this stage, accumulating

425   eolian systems tend to be dominated by sandsheets, associated with intermittent high-speed

426   wind conditions (Clemmensen, 1991), and by relatively thin dune sets, produced by the

427   repeated cannibalization of trains of dunes climbing at relatively low angles (Fig. 10A;

428   Mountney, 2006). Thus, sandsheets are expected to form a significantly greater percentage

429   (20% vs 12%) of observed icehouse eolian elements, relative to greenhouse successions.

430   As glacial conditions continue (at a time equivalent to that of the lowstand systems tract; cf.

431   Van Wagoner et al., 1990), the increasing aridity drives a further lowering of the water table

432   and the progressive loss of vegetation (in eolian systems deposited after the evolution of

433   vascular land plants). This leads to the exposure of even larger sediment volumes, which are

434   made available for entrainment and transport by strong trade winds with high sediment-

435   carrying capacities (Kocurek, 1998). The relative increase in aridity and windiness controls

436   both the availability of sediment for eolian transport and the transport capacity of the wind

437   (Fig. 2; cf. Sarnthein 1978; Anton 1983; Mainguet and Chemin 1983; Lancaster 1989, 1990;

438   Kocurek and Lancaster, 1999). Given these conditions, eolian sediment transport (flux) is

439   large. As sand-saturated air decelerates within a sedimentary basin in which unfilled

440   accommodation is available, large volumes of sand may be deposited rapidly; this promotes

441   the accumulation of thicker dune-sets, relative to those deposited at the onset of an eolian

442   accumulation episode (Fig. 10B; Wilson, 1971, 1973; Middleton and Southard, 1984;

443   Kocurek, 1991; Mountney, 2006). However, the ultimate preservation potential of these

444   thicker dune-sets may be relatively limited (see below).

445   As a glacial episode continues further, the upwind supply of sand is eventually exhausted

446   (Loope, 1985; Mountney, 2006). An upwind exhaustion of the sediment supply results in the

447   under-saturation of the airflow with respect to its potential sand-carrying capacity. This, in

448   combination with the highly erosive trade winds (which can be up to 60% more erosive than

449   they are under greenhouse conditions; Fig. 2; Kidder and Worsley, 2010, 2012) causes a

450   switch to net deflationary conditions around a time of maximum aridity when water tables are

451   low (Fig. 10C; Loope, 1985; Rubin and Hunter, 1982; Kocurek and Havholm, 1993;

452   Kocurek, 1999). Erosional conditions result in the commencement of erg deflation and

453   destruction (Wilson, 1973; Pye and Lancaster, 2009; Mountney, 2006; Bállico et al., 2017).

454   During the initial phase of glacial waning and associated onset of marine transgression, eolian

455   deflation of the dune-sets comprising the uppermost units of an accumulated eolian

456   succession continues (Fig. 10D; timing equivalent to that of the transgressive systems tract;

457 cf. Van Wagoner et al., 1990). The onset of interglacial conditions is associated with a

458 relative rise in sea level, a rise in the water table and re-colonization of the accumulation

459 surface by vegetation. Cumulatively, these factors, in combination with weakened trade-wind

460 strengths, reduce the volume of sediment susceptible to deflation, and the sediment transport

461 capacity of the wind (Kocurek, 1991; Mountney, 2006). Water tables rise above the level of

462 the thin dune sets and sandsheet deposits forming the lower parts of glacial eolian successions

463 (Fig. 10D), thereby enhancing their long-term preservation potential.

464 As the interglacial proceeds (timing equivalent to that of the highstand systems tract; cf. Van

465 Wagoner et al., 1990), the strength of trade winds continues to decrease (Fig. 2). The overall

466 reduction in both sediment-transport capacity and sediment supply rates make interglacial

467 eolian systems both supply- and transport-limited (cf. Kocurek and Lancaster, 1999).

468 Deflation progresses to the level of the water table (Stokes, 1968), generating a supersurface

469 (equivalent to a sequence boundary; cf. Van Wagoner et al., 1990), potentially associated

470 with surface stabilization resulting from colonization by vegetation or microbial

471 communities, by chemical precipitates, or by fluvial inundation (Fig. 10D; Loope, 1988;

472 Kocurek, 1991; Dott, 2003; Basilici et al., 2009, 2020; Eriksson et al., 2000; Dal' Bo et al.,

473 2010; Simpson et al., 2013). The timing of eolian supersurface formation can span a

474 protracted length of time, and its culmination can vary in timing from late in a glacial episode

475 to a point of maximum humidity during an ensuing interglacial episode (i.e. associated with

476 the highstand systems tract). Thus, the timing of supersurface formation may contrast with

477 that of sequence boundary formation in marine environments, which typically occurs during

478 the falling-stage and early lowstand systems tracts (cf. Mitchum, 1977).

479 As the interglacial continues, eolian accumulation remains limited. This is due to the

480 cumulative effects of elevated water tables and increased vegetation cover (in eolian systems

481 deposited after the evolution of vascular land plants), which act to limit sediment availability

482 (Fryberger et al., 1990; Kocurek and Havholm, 1993; Kidder and Worsley, 2010), and

483 weaker wind strengths, which act to limit sediment transport capacity (Kocurek, 1999). This

484 cycle of eolian accumulation recommences when climatic conditions tip back into windier,

485 more arid glacial conditions (Fig. 10E-G).

486 The process of deflation preferentially erodes the lager dune sets occurring in the upper part

487 of eolian successions that accumulated during glacial episodes; the thinner dune-sets and

488 sandsheets forming the lower parts of such successions are less prone to deflation, since the

489 concomitant rise in the water table can lead to their permanent preservation in the

490 stratigraphic record (Fig. 10D; Kocurek and Havholm, 1993; Mountney and Russell, 2009;

491 Mountney 2006). The preservation of relatively thicker dune-sets, associated with peak

492 aridity during glacial times, may be limited to times and tectonic contexts of rapid

493 subsidence. On the basis of this evolutionary model, the significantly reduced thickness of

494 icehouse – relative to greenhouse – eolian architectural elements (i.e. dune-sets, sandsheets

495 and interdunes) in the geological record is explained by their reduced preservation potential

496 over Milankovitch timescales (100-400 kyr).

497 *Icehouse Deflation*

498 During icehouse glacial episodes, generally more arid landscapes are associated with

499 relatively depressed water tables. As such, accumulating eolian successions are less likely to

500 be permanently sequestered beneath the water table, and are therefore prone to deflation by

501 strengthened low-latitude trade winds (Kocurek and Havholm, 1993). Such episodes are also

502 generally associated with a reduced presence of stabilizing agents on the Earth's surface (e.g.,

503 vegetation and biogenic and evaporitic crusts), leaving eolian deposits exposed to potential

504 erosion (Loope, 1988; Kocurek, 1991; Basilici et al., 2009, 2020; Dal' Bo et al., 2010).

505   The propensity of icehouse conditions to drive significant wind erosion following the

506   cessation of eolian accumulation is supported by the dominance of deflationary

507   supersurfaces, which are more common under icehouse conditions, relative to greenhouse

508   conditions (deflationary supersurfaces represent 88% and 67% of classified supersurfaces in

509   icehouse and greenhouse systems, respectively). The formation of deflationary supersurfaces

510   with associated wet-surface features indicates that conditions of net accumulation are related

511   to cyclic changes to net-erosional conditions, associated with eolian cannibalization and

512   deflation down to the water table (Stokes, 1968; Loope, 1985; Mountney and Jagger, 2004;

513   Mountney, 2006). This is the case for the icehouse Cedar Mesa Sandstone and many other

514   Permo-Carboniferous deposits across North America, in which erg sequences are capped by

515   regionally extensive deflationary, supersurfaces with associated sedimentary structures that

516   indicate deflation to the paleo-water table (Loope, 1985; Fryberger, 1993; Mountney and

517   Jagger, 2004; Mountney, 2006).

518   Greater rates of eolian winnowing under icehouse conditions are indicated by the higher

519   number of observations of sandsheet elements. Sandsheets can represent remnants of eroded

520   landforms of originally higher relief; their occurrence can reflect eolian deflation, whereby

521   the winnowing of finer-grained sand leaves behind a coarser lag (Nielsen and Kocurek, 1986;

522   Pye and Tsoar, 1990; Mountney and Russell, 2004, 2006). It is therefore significant that

523   deflationary lag strata form a common facies type in icehouse sandsheet deposits, but are a

524   comparatively rare component of greenhouse sandsheet deposits. The evidence of heightened

525   eolian deflation of sandsheets accumulated under icehouse conditions suggests that in this

526   global climate regime the cannibalization of eolian deposits was more common, in accord

527   with the preservation of relatively thinner eolian architectural elements (dune sets,

528   sandsheets, interdunes). The preferential cannibalization of eolian systems under icehouse

529 conditions indicates a propensity for these systems to develop a negative sediment budget

530 (likely due to exhaustion of an upwind eolian sediment supply).

531 The greater propensity for icehouse eolian systems to experience post-depositional deflation

532 is supported by the textural analysis of icehouse and greenhouse deposits. Overall, analysis of

533 sediment textures reveals that icehouse deposits are less texturally mature, have higher mean

534 values of modal grain sizes, are relatively more poorly sorted, and have grains that are

535 significantly more angular. The reduced textural maturity of icehouse sediments may be

536 attributed to the relatively coarse and angular nature of grains that constitute a winnowed lag

537 left being during the development of sandsheet elements (Nielsen and Kocurek, 1986; Pye

538 and Tsoar, 1990; Mountney and Russell, 2004, 2006). However, the differences in grain size

539 and sorting are not sufficiently large to be considered statistically significant; this finding is

540 congruous with the highly discriminant nature of sediment transport by wind (Bagnold,

541 1941), which may generate a relatively well-sorted sediment source prior to deflation.

542 **Greenhouse Conditions**

543 The fact that dune-set, sandsheet and interdune architectural elements are significantly thicker

544 in successions accumulated under greenhouse conditions, relative to those relating to

545 icehouse conditions (Fig. 4) is attributed to their greater preservation potential over 100-400

546 kyr timescales. Relative to icehouse conditions, greenhouse Earth provides favorable

547 conditions for the rapid incorporation of eolian elements into the geological record.

548 Greenhouse conditions are associated with high eustatic levels and more-humid conditions,

549 which generally promote elevated water tables situated close to the accumulation surface

550 (Kocurek et al., 2001; Cowling, 2016).

551 Although the greenhouse geological record testifies to temporal variations in humidity (e.g.,

552 Sames et al., 2020), the greenhouse Earth did not generally experience large-magnitude shifts

553 in global climate, relative to the glacial-interglacial oscillations of icehouse periods. As such,

554 greenhouse conditions are generally associated with consistently elevated water tables, which

555 experience only minor temporal changes in elevation relative to the accumulation surface

556 (Fig. 11). Consistently elevated water tables can effectively sequester eolian successions;

557 accumulating eolian successions are rapidly buried beneath the level of the water table, in

558 response to progressive but gradual subsidence, and are accordingly protected from potential

559 deflation by the wind, leading to the long-term accumulation of eolian systems (Fig. 11;

560 Kocurek and Havholm, 1993; Mountney and Russell, 2009). Elevated water-table conditions

561 are supported by the greater proportion of 'wet' interdune and 'sabkha' elements in

562 greenhouse eolian successions (Evans, et al., 1964; Purser and Evans, 1973; Fryberger et al.,

563 1990; Kocurek and Havholm, 1993; Garcia-Hidlago, 2002).

564 Elevated water tables interact with the accumulation surface to generate damp and wet

565 substrates that inhibit the deflation of eolian sand deposits; greater threshold velocities are

566 required to entrain wet or damp sand due to capillary water tension (Chepil, 1956; Bisal and

567 Hsieh, 1966; Azizov, 1977). Humid, shallow water-table conditions may also promote the

568 colonization of eolian substrates by vegetation or biogenic films or crusts in some

569 paleoenvironmental settings (Basilici et al., 2020). Vegetation can limit the mobility of

570 channelized river systems, which can potentially erode contiguous adjacent eolian deposits

571 (Davies and Gibling, 2010; Reis et al., 2020; Santos et al., 2017, 2020). Moreover, vegetation

572 can play a crucial role in dune construction and stabilization; vegetation disrupts primary

573 airflows in the near-surface layer, decelerating winds and leading to the fall-out from the

574 airflow of airborne sand grains (Kocurek and Nielsen, 1986), thereby promoting deposition;

575 once deposited, vegetation can effectively trap eolian sediment, protecting it from re-

576 suspension and potential erosion (Byrne and McCann, 1990; Ruz and Allard, 1994). The

577 precipitation of early diagenetic cements around plant-root structures in eolian sand can

578 further stabilize eolian surfaces (Mountney 2006).

579 The role of vegetation is only relevant for icehouse and greenhouse systems deposited after

580 ca. 420 Ma, when vascular land plants became widespread (Gifford and Foster, 1989;

581 Rainbird, 1992; Long, 2006; Davies and Gibling, 2010). However, the statistically significant

582 difference in mean eolian architectural element thickness for icehouse and greenhouse

583 conditions is also present in pre-vegetation Precambrian settings (see section *'Precambrian*

584 *Supercontinent').* It can therefore be inferred that vegetation may play a contributing, but not

585 crucial, role in determining eolian element thickness. Prior to the evolution of land plants,

586 other biotic stabilizing agents likely played a role in limiting eolian winnowing, notably the

587 presence of microbial films and crusts (e.g., Basilici et al., 2020).

588 The inference of the role played by stabilizing agents and higher water tables in minimizing

589 eolian deflation is supported by the nature of supersurfaces seen in greenhouse systems,

590 which are less likely to be deflationary than those formed under icehouse conditions (Fig.

591 7A). Greenhouse supersurfaces may be more likely to develop due to changes in depositional

592 environment, such as fluvial inundation (Fig. 11), or the development of sabkha elements.

593 The close proximity of the water table to the surface is interpreted to result in more closely

594 spaced supersurfaces in greenhouse eolian successions.

595 **Non-Eolian Elements**

596 Non-eolian elements, which interdigitate with eolian elements to varying degrees, and which

597 form over a third of all recorded element types by number of occurrences (comprising 37%

598 and 38% of icehouse and greenhouse successions, respectively) in otherwise eolian-

599 dominated successions, do not show a statistically significant difference in mean thickness

600 between icehouse and greenhouse conditions. This might indicate that, within dominantly

601 eolian systems, the thicknesses of interdigitated non-eolian elements are not primarily

602 controlled by factors that are inherent to icehouse and greenhouse climatic conditions. This

603 supports the idea that variations in eolian element thicknesses noted between icehouse and

604 greenhouse systems are largely due to the effects of changes in wind strength as a driver of

605 eolian accumulation and deflation. Many non-eolian elements are associated, to varying

606 degrees, with deposition in aqueous environments and are therefore unaffected or slightly

607 affected by changes in wind speed, strength and erosive power.

608 **Other Boundary Conditions**

609 *Supercontinental Setting*

610 The paleogeographic configuration and distribution of land masses has influenced sea level,

611 global temperatures and patterns of atmospheric circulation. Only two paleogeographic states

612 have existed in Earth history than spanned both icehouse and greenhouse conditions: the

613 Precambrian and Pangean supercontinental configurations. When icehouse and greenhouse

614 conditions are separately compared for these two supercontinental settings, the same

615 statistical differences in eolian element thicknesses persist, such that eolian deposits

616 associated with icehouse conditions are significantly thinner than those associated with

617 greenhouse conditions. This suggests that the prevailing global climate regime may have

618 influenced the development and preservation of eolian systems across different

619 supercontinental configurations. The Precambrian and Pangean supercontinents are

620 considered below.

621 ***Precambrian Supercontinents*** Evidence of Precambrian glaciogenic deposits have

622 been recorded from many continental land masses, including those originally placed at

623 tropical paleolatitudes (Shrag, 2002; Kirschvink, 1992). Precambrian icehouse conditions are

624 attributed to attenuated solar luminosity, the albedo caused by continental landmasses located

625   at low-latitudes, and relatively low levels of atmospheric carbon dioxide (Hoffman et al.,

626   1998; Kirschvink, 1992).

627   In rocks of Precambrian age, icehouse eolian deposits are significantly thinner relative to

628   their greenhouse counterparts (Fig. 8A). Changes in the strength and erosive power of the

629   trade winds are likely equally relevant for eolian deposits of Precambrian age, as Hadley cell

630   circulation is shown to have been active since the Proterozoic (Hoffman and Grotzinger,

631   1993). As such, the greater strength and erosive power of icehouse winds (Fig. 2) may be

632   responsible for enhanced winnowing and deflation of Precambrian icehouse eolian

633   architectural elements. Precambrian icehouse conditions are considered to have been amongst

634   the most extreme of all recorded icehouse periods; wind strength and erosive power are

635   interpreted to have been amongst the highest in Earth history (Fig. 2; Kirschvink, 1992; Allen

636   and Hoffman, 2005).

637   Several of the studied Precambrian successions are associated with deposition in intracratonic

638   basins, which are preferentially developed in the interiors of stable ancient cratons (e.g.,

639   Shaw et al., 1991; Aspler and Chiarenzelli, 1997; Deb and Pal, 2015), and which act as sites

640   where relatively thin eolian elements can accumulate and be preserved, through episodic

641   deposition between long periods of sediment bypass, controlled in part by relatively slow

642   rates of subsidence and accommodation generation (e.g., Bethke, 1985; Aspler and

643   Chiarenzelli, 1997). However, the differences in eolian element thickness between icehouse

644   and greenhouse successions cannot be ascribed to the basin setting that hosts them (Fig. 12).

645   In this study, greenhouse Precambrian deposits are all associated with accumulation in

646   intracratonic basins, however, their icehouse counterparts are largely associated with

647   deposition in continental rift and peripheral foreland basin settings; Fig. 12). Even though a

648   bias in this study exists whereby the studied Precambrian greenhouse eolian deposits were all

649   deposited in slowly subsiding intracratonic basins, the elements that make up these deposits

650   are still significantly thicker than their Precambrian icehouse counterparts (Fig. 8A). This

651   suggests that the climatic influence on eolian element thickness overrides the potential

652   control on preservation of accommodation generation and basin morphology.

653   ***Pangean Supercontinent*** The Late Paleozoic is associated with a transition from

654   icehouse to greenhouse conditions and changes in global atmospheric circulation (e.g.,

655   Rowley et al., 1985; Cecil, 1990; Parrish, 1993; West et al., 1997; Gibbs et al., 2002). The

656   Late Paleozoic global climate change was closely associated with the formation of the

657   Pangean supercontinent. The assemblage of Pangea resulted in the aggregation of large

658   volumes of continental landmasses centered on the South Pole (Smith et al., 1973;

659   McElhinny et al., 1981; Ziegler et al., 1983), which experienced widespread continental

660   glaciation from ca. 360 to 300 Ma. The spread of continental glaciation was halted by

661   increasing levels of atmospheric carbon dioxide and the northward drift of the continents:

662   after ca. 300 Ma, the Earth tipped back into greenhouse climatic conditions (Parrish, 1993).

663   The Pangean supercontinent disrupted zonal atmospheric circulation, leading to the

664   development of the Pangean megamonsoon, which is comparable to the East Asian Monsoon

665   and was characterized by a seasonal reversal of winds (Kutzbach and Gallimore, 1989;

666   Parrish, 1993). The megamonsoon was active in the Permian, intensified into the Triassic,

667   and continued on the Gondwanan supercontinent until the beginning of the Cretaceous

668   (Parrish, 1993; Scherer and Goldberg, 2007; Scherer et al., 2020).

669   The megamonsoon and its associated seasonal reversals in wind direction are widely

670   documented in the eolian record and have likely influenced the architecture of eolian deposits

671   (e.g., Loope et al., 2001). It can thus be hypothesized that the megamonsoon may have also

672   governed accumulated eolian element thickness, perhaps in a way that would have

673   overprinted the effects of the controls exerted by icehouse and greenhouse conditions.

674   However, despite the additional control imposed by megamonsoon conditions, icehouse

675　eolian architectural elements (i.e. dune-sets, sandsheets and interdunes) remain significantly

676　thinner than greenhouse architectural elements in stratigraphies of this age (Fig. 8A).

677　Moreover, the mean thickness of greenhouse Pangean architectural elements (i.e. those

678　deposited under peak megamonsoon conditions) does not differ significantly from

679　greenhouse architectural elements deposited under comparable supercontinental settings (Fig.

680　13; Table 3). The impact of the megamonsoon on accumulated eolian element thickness is

681　therefore considered to have been secondary compared to the climatic influence of icehouse-

682　greenhouse oscillations. However, a limitation exists in this analysis, since icehouse

683　conditions only prevailed on Pangea during its initial accretion, and the Pangean climate was

684　dominated by greenhouse conditions for the majority of its existence.

685　*Basin Configuration*

686　The long-term preservation of eolian systems in the geological record requires the

687　development of accommodation in which eolian deposits can accumulate. The basin

688　morphology and rate of accommodation generation varies significantly between the basin

689　types considered here (intracratonic, rift and foreland basins; see Table 2). Despite this,

690　statistical differences between the thicknesses of icehouse and greenhouse architectural

691　elements are noted for all basin types considered in this study (Fig. 8B), whereby eolian

692　architectural elements associated with icehouse periods are significantly thinner than those of

693　greenhouse periods. This suggests that the climatic influence on eolian element thickness

694　overrides the potential controls of accommodation generation and basin morphology.

695　*Paleolatitude*

696　The preserved architecture of eolian systems is influenced by the latitude at which the eolian

697　systems developed (Fig. 8C). The existence of the icehouse/greenhouse signature at low

698　latitudes (<30°), and the absence of this signature at higher latitudes (>30°), supports the

699   previous assertion that the differences in eolian element thicknesses are governed by

700   atmospheric circulation at low latitudes, caused by icehouse/greenhouse modulation of the

701   Hadley circulation, and associated with changes in the strength of the trade winds (Chandler,

702   1992; Lu et al., 2007; Hasegawa et al., 2011). Outside the zone of influence of the trade

703   winds (>30° latitude), the icehouse-greenhouse signature is apparently not evident in the

704   geological record; this suggests that the effects of global climate oscillations are overprinted

705   by other forcing mechanisms in that context, such as rate and type of sediment supply,

706   tectonic configuration, basin setting and dune-field physiographic setting.

707   *Dune-field (Erg) Physiographic Setting*

708   Across the different dune-field settings of eolian sand seas (i.e. back, center and fore erg-

709   settings), variations in eolian element thickness are seen, with central-erg eolian architectural-

710   elements being on average thicker than fore- and back-erg elements. However, across all

711   environments of eolian sand seas, statistically significant differences in eolian architectural

712   element thickness are seen between icehouse and greenhouse successions, such that icehouse

713   eolian elements are consistently thinner relative to greenhouse architectural elements (Fig.

714   8D). The fact that this difference is seen across all dune-field physiographic settings

715   corroborates the idea that the differences in eolian element thickness are the result of large-

716   scale circulation patterns, which overprint signatures associated with localized and autogenic

717   controls.

718   **CONCLUSIONS**

719   The continental terrestrial record has here been shown to preserve a valuable archive of how

720   ancient sedimentary systems respond to and record changes in global climate. This study

721   provides the first integrated global-scale quantitative investigation into the effects of climatic

722   oscillations on eolian sedimentary architecture. More than >5,600 geological entities

723   extracted from 34 case studies, spanning a variety of spatio-temporal settings, have been

724   analyzed (Fig. 1). Icehouse and greenhouse conditions exert a fundamental and statistically

725   detectable influence on preserved eolian dune-set, sandsheet and interdune thicknesses (Fig.

726   4; Table 3), such that icehouse eolian architectural elements are significantly thinner than

727   greenhouse architectural elements. This statistical signature is present regardless of (i) basin

728   type, (ii) paleogeographic configuration, and (iii) dune-field (erg) physiographic setting (Fig.

729   8; Table 3). However, the icehouse-greenhouse signature is only present at paleolatitudes

730   <30°; it is absent in systems from higher paleolatitudes (Fig. 8C). Differences in eolian

731   element thicknesses are interpreted in terms of changes in the pattern of circulation of low-

732   latitude trade winds (Fig. 2), which operate at latitudes <30°.

733   Under icehouse conditions, Milankovitch-driven cycles of eolian accumulation and deflation

734   result in the preservation of thin eolian architectural elements (i.e. dune sets, sandsheets and

735   interdunes Figs. 4, 10); as an icehouse glacial initiates, thin dune sets and sandsheets are

736   deposited under high wind strengths. As the glacial proceeds, higher trade-wind strengths

737   result in the deposition of relatively thicker dune-sets, until upwind sources are exhausted

738   (Fig. 10). The thick glacial dune-sets have limited preservation potential due to depressed

739   water tables and the highly erosive nature of the strengthened trade winds. During interglacial

740   periods, relative rises in the water-table enable the preservation of the thin basal dune-sets

741   and sandsheets (Fig. 10).

742   Relative to greenhouse conditions, icehouse conditions are also associated with (i) a greater

743   proportion of deflation-lag facies in sandsheet and interdune elements; (ii) relatively more

744   observations of sandsheet strata, indicative of higher wind strengths; and (iii) a higher

745   proportion of deflationary supersurfaces (Fig. 7). Consistently and significantly thicker

746   greenhouse deposits are attributed to relatively elevated water tables (associated with wet

747   interdunes and sabkha elements), which exhibit only minor temporal variations in level

748 relative to the accumulation surface, and enhanced surface stabilization by vegetation or other

749 biotic agents, all of which inhibit eolian deflation. Relative to icehouse conditions,

750 greenhouse conditions are associated with: (i) eolian architectures dominated by an increased

751 occurrence of dune-set elements, with fewer recorded sandsheet and interdune elements (Fig.

752 3B); (ii) interdunes that, where present, are more likely to be of a damp or wet type (Fig. 5A);

753 (iii) a greater proportion of interdigitating sabkha elements (Fig. 3C).

754 This study presents a quantitative assessment of how the influence of icehouse and

755 greenhouse climates on Earth surface processes is archived in the continental stratigraphic

756 record. The results presented here provide novel insights into the fundamental boundary

757 conditions that govern eolian sedimentary architectures, and have been used to develop

758 idealized eolian icehouse and greenhouse facies models based on the most likely association

759 of eolian and associated non-eolian architectural elements and bounding surfaces. The

760 architectures of low-latitude eolian systems are fundamentally influenced by the prevailing

761 global climate, and the way this influence has been translated into the stratigraphic record has

762 been consistent through geological time. Results presented here help quantify and understand

763 sedimentary responses to fundamental processes that operate on the surface of the Earth as a

764 consequence of changes in global climate. In the context of human-induced climate change,

765 these findings may be valuable for future predictions of the response of the terrestrial

766 geosphere to fundamental changes in global climate.

767

772 (now Orano), BHPBilliton, Cairn India (Vedanta), ConocoPhillips, Chevron, Equinor,

773 Murphy Oil, CNOOC, Occidental, Petrotechnical Data Systems, Saudi Aramco, Shell,

774 Tullow Oil, Woodside and YPF.

775

776

777 **REFERENCES**

778 Ager, D.V., 1993, The Nature of the Stratigraphical Record, 3rd edn. John Wiley & Sons,

779 Chichester, New York, Brisbane, Toronto, Singapore, 151 pp.

780

781 Ahlbrandt, T.S., Andrews, S. and Gwynne, D.T., 1978, Bioturbation in eolian deposits,

782 Journal of Sedimentary Petrology, v. 48, p. 839–848.

783 doi.org/10.1306/212F7586-2B24-11D7-8648000102C1865D

784

785 Allen, J.R.L., 1963, The classification of cross-stratified units with notes on their origin,

786 Sedimentology, v. 2, p. 93–114.

787 doi.org/10.1111/j.1365-3091.1963.tb01204.x

788

789 Andrew, R. M., A comparison of estimates of global carbon dioxide emissions from fossil

790 carbon sources, Earth System Science Data, v. 12, p. 1437–1465,

791 doi.org/10.5194/essd-12-1437-2020, 2020.

792

793 Andreucci, S., Clemmensen, L.B. and Pascucci, V., 2010, Transgressive dune formation

794 along a cliffed coast at 75ka in Sardinia, Western Mediterranean: a record of sea-level fall

795 and increased windiness. Terra Nova, v. 22, p. 424–433.

796 doi.org/10.1111/j.1365-3121.2010.00971.x

797

798 Anton, D., 1983, Modern eolian deposits of the eastern province of Saudi Arabia, in

799 Brookfield, M.E. and Ahlbrandt, T.S., Eolian Sediments and Processes, Developments in

800 Sedimentology, v. 38, p. 365-378.

801 doi.org/10.1016/S0070-4571(08)70805-7

802

803 Aspler, L.B. and Chiarenzelli, J.R., 1997, Initiation of 2.45–2.1 Ga intracratonic basin

804 sedimentation of the Hurwitz Group, Keewatin Hinterland, Northwest Territories, Canada,

805 Precambrian Research, v. 81, p. 265-297.

806 doi.org/10.1016/S0301-9268(96)00038-1

807

808 Atchley, S.C. and Loope, D.B., 1993, Low-stand aeolian influence on stratigraphic

809 completeness: upper member of the Hermosa Formation (latest Carboniferous), southeast

810 Utah, USA. In Pye, K. and Lancaster, N., Aeolian Sediments: Ancient and Modern, 127 –

811 149 pp.

812   doi.org/10.1002/9781444303971.ch9

813

814 Azizov, A., 1977, Influence of soil moisture on the resistance of soil to wind erosion, Soviet

815 Soil Science, v. 9, p. 105-108. ISSN: 0038-5832

816

817 Bagnold, R.A., 1941, The physics of blown sand and desert dunes, London: Methuen.

818

819 Bállico, M.B., Scherer, C.M.S., Mountney, N.P., Souza, E.G., Chemale, F., Pisarevsky, S.A.

820 and Reis A.D., 2017, Wind-pattern circulation as a palaeogeographic indicator: Case study of

821   the 1.5-1.6 Ga Mangabeira Formation, Sao Francisco Craton, Northeast Brazil, Precambrian

822   Research, v. 298, p. 1-15.

823   doi.org/10.1016/j.precamres.2017.05.005

824

825   Bart, H.A., 1977, Sedimentology of cross-stratified sandstones in Arikaree Group, Miocene,

826   Southeastern Wyoming, Sedimentary Geology, v. 19, p. 165-184.

827   doi.org/10.1016/0037-0738(77)90029-X

828

829   Basilici, G., Dal' Bo, P.F.F. and Ladeira, F.S.B., 2009, Climate-induced sediment-palaeosol

830   cycles in a Late Cretaceous dry aeolian sand sheet: Marília Formation (North-West Bauru

831   Basin, Brazil), Sedimentology, v. 56, p. 1876-1904.

832   doi.org/10.1111/j.1365-3091.2009.01061.x

833

834   Basilici, G., Vinicius, M., Soares, T., Mountney, N.P., Colombera, L., 2020, Microbial

835   influence on the accumulation of Precambrian aeolian deposits (Neoproterozoic, Venkatpur

836   Sandstone Formation, Southern India), Precambrian Research, v. 347, 105854.

837   doi.org/10.1016/j.precamres.2020.105854

838

839   Benan, C.A.A. and Kocurek, G., 2000, Catastrophic flooding of an aeolian dune field:

840   Jurassic Entrada and Todilto Formations, Ghost Ranch, New Mexico, USA, Sedimentology,

841   v. 47, p. 1069-1080.

842   doi.org/10.1046/j.1365-3091.2000.00341.x

843

844 Bethke, C.M., 1985, A numerical model of compaction-driven groundwater flow and heat

845 transfer and its application to the paleohydrology of intracratonic sedimentary basins, Journal

846 of Solid Earth, v. 90, p. 6817-6828.

847 doi.org/10.1029/JB090iB08p06817

848

849 Bisal, F. and Hsieh, J., 1966, Influence of moisture on erodibility of soil by wind, Soil

850 Science, v. 102, p. 143-146.

851

852 Biswas, A., 2005, Coarse aeolianites: sand sheets and zibar-interzibar facies from the

853 Mesoproterozoic Cuddapah Basin, India, Sedimentary Geology, v. 174, p. 149-160.

854 doi.org/10.1016/j.sedgeo.2004.11.005

855

856 Blakey, R.C., 1988, Basin tectonics and erg response, Sedimentary Geology, v. 56, p. 127-

857 151. doi.org/10.1016/0037-0738(88)90051-6

858

859 Blakey, R.C. and Middleton, L.T., 1983, Permian shoreline eolian complex in central

860 Arizona: dune changes in response to cyclic sea-level changes, in Brookfield, M.E and

861 Ahlbrandt, T.S., eds., Eolian Sediments and Processes, Developments in Sedimentology,

862 v.38, p. 551–581. Elsevier, Amsterdam.

863 doi.org/10.1016/S0070-4571(08)70813-6

864

865 Bowring, S., Myrow, P., Landing, E., Ramezani, J., and Grotzinger, J., 2003,

866 Geochronological constraints on terminal Neoproterozoic events and the rise of

867 Metazoans, Geophysical Research Abstracts, v. 5, 13,219. EGS - AGU - EUG Joint

868   Assembly, Abstracts from the meeting held in Nice, France, 6 - 11 April 2003, abstract id.

869   13219

870

871   Breed, C.S. and Grow, T., 1979, Morphology and distribution of dunes in sand seas observed

872   by remote sensing, in McKee, E.D., ed., A study of global sand seas, U.S. Government

873   Printing Office, Washington, DC, pp 253–302.

874

875   Brenchley, P.J., Marshall, J. D., Carden, G.A.F., Robertson, D.B.R., Long, D.G.F., Meidla,

876   T., Hints, L. and Anderson. T.F., 1994, Bathymetric and isotopic evidence for a short-lived

877   Late Ordovician glaciation in a greenhouse period, Geology, v. 22, p. 295–29.

878   doi.org/10.1130/0091-7613(1994)022<0295:BAIEFA>2.3.CO;2

879

880   Bristow, C.S. and Mountney, N.P., 2013, Aeolian Landscapes, Aeolian Stratigraphy, in

881   Shroder, J., ed., Treatise on Geomorphology, pp. 246-268. Elsevier, San Diegeo, USA

882

883   Brooke, B., 2001, The distribution of carbonate eolianite. Earth-Science Reviews, v. 55, p.

884   135–164.

885   doi.org/10.1016/S0012-8252(01)00054-X

886

887   Brookfield, M.E., 1977, The origin of bounding surfaces in ancient aeolian sandstones,

888   Sedimentology, v. 24, p. 303-332.

889   doi.org/10.1111/j.1365-3091.1977.tb00126.x

890

891   Brookfield, M.E., 1992, Eolian systems, in Walker, R.G. and James, N.P., Facies Models.

892   Response to Sea Level Change, Geological Association of Canada, pp. 143–156.

893

894 Byrne, M.-L. and McCann, S.B., 1989, Stratification models for vegetated coastal dunes in

895 Atlantic Canada, Sedimentary Geology, v. 66, p. 165-179.

896 doi.org/10.1016/0037-0738(90)90058-2

897

898 Cather, S.M., Connell, S.D., Chamberlin, R.M., McIntosh, W.C., Jones, G.E., Potochnik,

899 A.R., Lucas, S.G. and Johnson, P.S., 2008, The Chuska erg: Paleogeomorphic and

900 paleoclimatic implications of an Oligocene sand sea on the Colorado Plateau, Geological

901 Society of America Bulletin, v. 120, p. 13-33.

902 doi.org/10.1130/B26081.1.

903

904 Cecil, C.B., 1990, Paleoclimate controls on stratigraphic repetition of chemical and

905 siliciclastic rocks, Geology, v. 18, p. 533–536.

906 doi.org/10.1130/0091-7613(1990)018<0533:PCOSRO>2.3.CO;2

907

908 Chan, M.A. and Kocurek, G., 1988, Complexities in eolian and marine interactions:

909 processes and eustatic controls on erg development, Sedimentary Geology, v. 56, p. 283-300.

910 doi.org/10.1016/0037-0738(88)90057-7

911

912 Chandler, M.A., Rind, D. and Ruedy, R., 1992, Pangaean climate during the Early Jurassic:

913 GCM simulations and the sedimentary record of paleoclimate, Geological Society of America

914 Bulletin, v. 104, p. 543-559.

915 doi.org/10.1130/0016-7606(1992)104<0543:PCDTEJ>2.3.CO;2

916

917   Chepil, W.S., 1956, Influence of moisture on erodibility of soil by wind, Soil Science Society

918   of America Proceedings, v. 20, p. 288-292.

919

920   Chrintz, T. and Clemmensen, L.B., 1993, Draa reconstruction, the Permian Yellow Sands,

921   northeast England, in Pye, K. and Lancaster, N., Aeolian sediments. Ancient and modern,

922   International Association of Sedimentologists Special Publication, v. 16, p. 151-161.

923   doi.org/10.1002/9781444303971.ch10

924

925   Clarke, M.L. and Rendell, H.M., 1998, Climate change impacts on sand supply and the

926   formation of desert sand dunes in the south-west U.S.A, Journal of Arid Environments, v. 39,

927   p. 517–531.

928   doi.org/10.1006/jare.1997.0372

929

930   Clemens, S. C., 1998, Dust response to seasonal atmospheric forcing: Proxy evaluation and

931   calibration, Paleoceanography, v. 13, p. 471–490.

932   doi.org/10.1029/98PA02131.

933

934   Clemmensen, L.B., 1985, Desert sand plain and sabkha deposits from the Bunter Sandstone

935   formation (L.Triassic) at the northern margin of the German Basin, Geologische Rundschau,

936   v. 74, p. 519-536.

937   doi.org/10.1007/BF01821209

938

939   Clemmensen, L.B., 1987, Complex star dunes and associated aeolian bedforms, Hopeman

940   Sandstone (Permo-Triassic), Moray Firth Basin, Scotland, in Frostick, L.E. and Reid, I.,

941 Desert Sediments: Ancient and Modern, Geological Society of London Special Publictaion,

942 35, p. 213-231.

943 doi.org/10.1144/GSL.SP.1987.035.01.15

944

945 Clemmensen, L.B., 1988, Aeolian morphology preserved by lava cover, the Precambrian

946 Mussartut Member, Eriksfjord Formation, South Greenland, Bulletin of the Geological

947 Society of Denmark, v. 37, p. 105-116.

948

949 Clemmensen L.B., 1991, Controls on aeolian sand sheet formation exemplified by the Lower

950 Triassic of Helgoland, in Barndorff-Nielsen O.E., Willetts B.B., eds, Aeolian Grain

951 Transport. Acta Mechanica Supplementum, v. 2. Springer, Vienna.

952 doi.org/10.1007/978-3-7091-6703-8_12

953

954 Clemmensen, L.B. and Abrahamsen, K., 1983, Aeolian stratification and facies association in

955 desert sediments, Arran basin (Permian), Scotland, Sedimentology, v. 30, p. 311-339.

956 doi.org/10.1111/j.1365-3091.1983.tb00676.x

957

958 Clemmensen, L.B. and Abrahansen, K., 1983, Aeolian stratification and facies association in

959 desert sediments, Arran Basin (Permian), Scotland, Sedimentology, v. 30, p. 311-339.

960 doi.org/10.1111/j.1365-3091.1983.tb00676.x

961

962 Clemmensen, L.B. and Blakey, R.C., 1989, Erg deposits in the Lower Jurassic Wingate

963 Sandstone, Northeastern Arizona: Oblique dune sedimentation, Sedimentology, v. 36, p. 449-

964 470.

965 doi.org/10.1111/j.1365-3091.1989.tb00619.x.

966

967 Clemmensen, L.B., Fornós, J.J. and Rodríguez-Perea, A., 1997, Morphology and architecture

968 of a late Pleistocene cliff-front dune, Mallorca, Western Mediterranean. Terra Nova, v. 9, p.

969 251–254.

970 doi.org/10.1111/j.1365-3121.1997.tb00023.x

971

972 Cojan, I. and Thiry, M., 1992, Seismically induced deformation structures in Oligocene

973 shallow-marine and aeolian coastal sands (Paris Basin), Tectonophysics, v. 206, p. 78-89.

974 doi.org/10.1016/0040-1951(92)90369-H

975

976 Coleman, A.P., 1907, A lower Huronian ice age. American Journal of Science, v. 23, p. 187–

977 192.

978

979 Colombera, L., Mountney, N.P. and McCaffrey, W.D., 2012, A relational database for the

980 digitization of fluvial architecture concepts and example applications, Petroleum Geoscience,

981 v. 18, p. 129-140.

982 doi.org/10.1144/1354-079311-021

983

984 Colombera, L., Mountney, N.P., Hodgson, D.M. and McCaffrey, W.D., 2016, The Shallow-

985 Marine Architecture Knowledge Store: A database for the characterization of shallow-marine

986 and paralic depositional systems, Marine and Petroleum Geology, v. 75, p. 83-99.

987 doi.org/10.1016/j.marpetgeo.2016.03.027

988

989 Cowan, G., 1993, Identification and significance of aeolian deposits within the dominantly

990 fluvial Sherwood Sandstone group of the East Irish Sea Basin UK, in North, C.P. and Prosser,

991   D.J., eds., Characterization of fluvial and aeolian reservoirs, Geological Society of London

992   Special Publication, v. 73, p. 231-245.

993   doi.org/10.1144/GSL.SP.1993.073.01.14

994

995   Cowling, S.A., 2016, Sea level and ground water table depth (WTD): A biogeochemical

996   pacemaker for glacial-interglacial cycling, Quaternary Science Reviews, v. 151, p. 309-314.

997   doi.org/10.1016/j.quascirev.2016.09.009

998

999   Crabaugh, M. and Kocurek, G., 1993, Entrada Sandstone: An example of a wet aeolian

1000   system, in Pye, K., ed., The dynamics and environmental context of aeolian sedimentary

1001   systems, Geological Society of London Special Publication, v. 72, p. 103-126.

1002   doi.org/10.1144/GSL.SP.1993.072.01.11

1003

1004   Crowell, J.C., 1999, Pre-Mesozoic Ice Ages: Their Bearing on Understanding the Climate

1005   System: Boulder, Colorado, Geological Society of America Memoir 192, p. 2-77.

1006   ISBN: 0813711924, 9780813711928

1007

1008   Dal' Bo, P.F.F., Basilici, G. and Angélica, R.S., 2010, Factors of paleosol formation in a Late

1009   Cretaceous eolian sand sheet paleoenvironment, Marília Formation, Southeastern Brazil,

1010   Palaeogeography, Palaeoclimatology and Palaeoecology, v. 292, p. 349-365.

1011   doi.org/10.1016/j.palaeo.2010.04.021

1012

1013   Dasgupta, P.K., Biswas, A. and Mukherjee, R., 2005, Cyclicity in Palaeoproterozoic to

1014   Neoproterozoic Cuddapah Supergroup and its significance in basinal evolution, in

1015   Mabesoone, J.M. and Neumann, V.H., Cyclic Development of Sedimentary Basins,

1016   Developments in Sedimentology, v. 57, p. 313-354.

1017   doi.org/10.1016/S0070-4571(05)80013-5

1018

1019   Davies, N.S. and Gibling, M.R., 2010, Cambrian to Devonian evolution of alluvial systems:

1020   The sedimentological impact of the earliest land plants, Earth Science Reviews, v. 98, p. 171-

1021   200.

1022   doi.org/10.1016/j.earscirev.2009.11.002

1023

1024   Deb, M. and Pal, T., 2015, Mineral potential of Proterozoic intracratonic basins in India, in:

1025   Mazumder, R. and Eriksson, P.G., eds., Precambrian Basins on India, Geological Society of

1026   London, Memoir, v. 43, p. 309-325.

1027   doi.org/10.1144/M43.21

1028

1029   Dias, K.D.N. and Scherer, C.M.S., 2008, Cross-bedding set thickness and stratigraphic

1030   architecture of aeolian systems: An example from the Upper Permian Piramboia Formation

1031   (Parana Basin), southern Brazil, Journal of South American Earth Sciences, v. 25, p. 405-415.

1032   doi.org/10.1016/j.jsames.2007.07.008

1033

1034   Dickinson, W.R., Soreghan, G.S. and Giles, K.A., 1994, Glacio-eustatic origin of Permo-

1035   carboniferous stratigraphic cycles: evidence from the southern Cordilleran foreland region, in

1036   Dennison, J.M. and Ettensohn, F.R., eds., Tectonic and Eustatic Controls on Sedimentary

1037   Cycles, Society for Sedimentary Geology Concepts in Sedimentology and Paleontology, v. 4,

1038   p. 25–34.

1039   doi.org/10.2110/csp.94.04.0025

1040

1041   Dott, R.H., Byers, C.W., Fielder, G.W., Stenzel, S.R. and Winfree, K.E., 1986, Aeolian to

1042   marine transition in Cambro-Ordovician cratonic sheet sandstones of the northern Mississippi

1043   valley, U.S.A, Sedimentology, v. 33, p. 345-367.

1044   doi.org/10.1111/j.1365-3091.1986.tb00541.x

1045

1046   Dott, Jr., R., 2003, The Importance of Eolian Abrasion in Supermature Quartz Sandstones

1047   and the Paradox of Weathering on Vegetation-Free Landscapes. The Journal of Geology, v.

1048   111, p. 387-405. doi:10.1086/375286

1049

1050   Einsele, G., 2013, Sedimentary Basins: Evolution, Facies and Sediment Budgets, Springer,

1051   New York, NY, p. 4.

1052   ISBN 978-3-662-04029-4

1053

1054   Ellis, D., 1993, The Rough Gas Field: distribution of Permian aeolian and non-aeolian

1055   reservoir facies and their impact on field development, Geological Society of London Special

1056   Publication 73, p. 265-277.

1057   doi.org/10.1144/GSL.SP.1993.073.01.16

1058

1059   Eriksson, K.A., McClung, W.S. and Simpson, E.L., 2019, Sequence stratigraphic expression

1060   of greenhouse, transitional and icehouse conditions in siliciclastic successions: Paleozoic

1061   examples from the central appalachian basin, USA, Earth Science Reviews, v. 188, p. 176 –

1062   189.

1063   doi.org/10.1016/j.earscirev.2018.11.010

1064

1065 Eriksson, P.G., Simpson, E.L., Eriksson, K.A., Bumby, A.J., Steyn, G.L. and Sarkar, S.,

1066 2000, Muddy Roll-up Structures in Siliciclastic Interdune Beds of the c. 1.8 Ga Waterberg

1067 Group, South Africa. PALAIOS, v. 15, p. 177–183.

1068 doi: https://doi.org/10.1669/0883-1351(2000)015<0177:MRUSIS>2.0.CO;2

1069

1070 Evans, G., Kendall., C.G.St.C. and Skipwith, P., 1964, Origin of coastal flats, the sabkha of

1071 the Trucial Coast, Persian Gulf, Nature, v. 202, p. 759-761.

1072 doi.org/10.1038/202759a0

1073

1074 Evans, D.A., Beukes, N.J., Kirschvink, J.L., 1997, Low-latitude glaciation in the

1075 Paleoproterozoic era, Nature v. 386, p. 262–266.

1076 doi.org/10.1038/386262a0.

1077

1078 Folk, R.L. and Ward, W.C., 1957, Brazos River bar: a study in the significance of grain size

1079 parameters, Journal of Sedimentary Petrology, v. 27, p. 3–26.

1080

1081 Formolo Ferronatto, J.P., dos Santos Scherer, C.M., de Souza, E.G, dos Reis, A.D. and de

1082 Mello, R.G., 2019, Genetic units and facies architecture of a Lower Cretaceous fluvial-

1083 aeolian succession, Sao Sebastiao Formation, Jatoba Basin, Brazil, Journal of South

1084 American Earth Sciences, v. 89, p. 158-172.

1085 doi.org/10.1016/j.jsames.2018.11.009

1086

1087 Fornós, J., Clemmensen, L.B., Gómez-Pujol, L. and Murray, A.S., 2009, Late Pleistocene

1088 carbonate aeolianites onMallorca, Western Mediterranean: a luminescencechronology.

1089 Quaternary Science Reviews, v. 28, p. 2697–2709.

1090   doi.org/10.1016/j.quascirev.2009.06.008

1091

1092   Forster A., Schouten S., Baas M. and Sinninghe Damsté J. S., 2007, Mid-Cretaceous (Albian-

1093   Santonian) sea surface temperature record of the tropical Atlantic Ocean, Geology, v. 35, p.

1094   919–922.

1095   doi.org.10.1130/G23874A.1

1096

1097   Frakes, L.A., Francis, J.E., and Syktus, J.I., 1992, Climate modes of the Phanerozoic, New

1098   York: Cambridge University Press, pp. 274.

1099

1100   Fryberger, S.G., 1993, A review of aeolian bounding surfaces, with examples from the

1101   Permian Minnelusa Formation, USA, in North, C.P. and Prosser, D.J., eds., Characterization

1102   of fluvial and aeolian reservoirs, Geological Society of London Special Publication 73,

1103   p.167-197. doi.org/10.1144/GSL.SP.1993.073.01.11.

1104

1105   Fryberger, S.G. and Schenk, C.J., 1988, Pin stripe lamination- a distinctive feature of modern

1106   and ancient eolian sediments, Sedimentary Geology, v. 55, p. 1-15.

1107   doi.org/10.1016/0037-0738(88)90087-5

1108

1109   Fryberger, S.G., Schenk, C.J. and Krystinik, L.F., 1988, Stokes surfaces and the effects of

1110   near-surface groundwater-table on Aeolian deposition, Sedimentology, v. 35, p. 21-41.

1111   doi.org/10.1111/j.1365-3091.1988.tb00903.x

1112

1113   Fryberger, S.G., Krystinik, L.F. and Schenk, C.J., 1990, Tidally flooded back-barrier

1114   dunefield, Guerrero Negro area, Baja California, Mexico, Sedimentology, v. 37, p. 23-43.

1115 doi.org/10.1111/j.1365-3091.1990.tb01981.x

1116

1117 García-Hidalgo, J.F., Temiño, J. and Segura, M., 2002, Holocene eolian sediments on the

1118 southern border of the Duero Basin (Spain): origin and development of an eolian system in a

1119 temperate zone, Journal of Sedimentary Research, v. 72, p. 30-39.

1120 doi.org/10.1306/040501720030

1121

1122 Gibbs, M.T., Rees, P.M., Kutzbach, J.E., Ziegler, A.M., Behling, P.J. and Rowley, D.B.,

1123 2002, Simulations of Permian climate and comparisons with climate-sensitive sediments, The

1124 Journal of Geology, v. 110, p. 33–55.

1125 doi.org/10.1086/324204

1126

1127 Glennie, K.W. and Buller, A.T., 1983, The Permian Weissliegend of North West Europe. The

1128 partial deformation of aeolian dune sands caused by the Zechstein transgression, Sedimentary

1129 Geology, v. 35, p. 43-81.

1130 doi.org/10.1016/0037-0738(83)90069-6

1131

1132 Goddéris, Y., Donnadieu, Y., Carretier, S., Aretz, M., Dera, G., Macouin, M. and Regard, V.,

1133 2017, Onset and ending of the late Palaeozoic ice age triggered by tectonically paced rock

1134 weathering, Nature Geoscience, v. 10, p. 382–386.

1135 doi.org/10.1038/ngeo2931.

1136

1137 Guern, P.L. and Davaud, E., 2005, Recognition of ancient carbonate wind deposits: lessons

1138 from a modern analogue, Chrissi Island, Crete. Sedimentology, v. 52, p. 915–926.

1139 doi.org/10.1111/j.1365-3091.2005.00700.x

1140

1141 Hasegawa, H., Tada, R., Jiang, X., Suganuma, Y., Imsamut, S., Charusiri, P., Ichinnorov, N.

1142 and Khand, Y., 2012, Drastic shrinking of the Hadley circulation during the mid-Cretaceous

1143 Supergreenhouse, Climate of the Past, v. 8, p. 1323-1337.

1144 doi.org/10.5194/cp-8-1323-2012.

1145

1146 Hodgson, D.M., Bernhardt, A., Clare, M.A., Da Silva, A-C., Fosdick Julie, C., Mauz, B.,

1147 Midtkandal, I., Owen, A., Romans, B.W., 2018, Grand Challenges (and Great Opportunities)

1148 in Sedimentology, Stratigraphy, and Diagenesis Research, Frontiers in Earth Science, v. 6, p.

1149 173

1150 Doi.org/10.3389/feart.2018.00173

1151

1152 Hoffman, P.F. and Grotzinger, 1993, Orographic precipitation, erosional unloading, and

1153 tectonic style, Geology, v. 21, p. 195-198.

1154 doi.org/10.1130/0091-7613(1993)021<0195:OPEUAT>2.3.CO;2

1155

1156 Hoffmann, K.-H., Condon, D.J., Bowring, S.A., and Crowley, J.L., 2004, U-Pb zircon date

1157 from the Neoproterozoic Ghaub Formation, Namibia: Constraints on Marinoan glaciation,

1158 Geology, v. 32, p. 817–820.

1159 doi.org/10.1130/G20519.1

1160

1161 Howell, J.A. and Mountney, N.P., 2001, Aeolian grain flow architecture: hard data for

1162 reservoir models and implications for red bed sequence stratigraphy, Petroleum Geoscience,

1163 v. 7, p. 51-56.

1164 doi.org/10.1144/petgeo.7.1.51

1165

1166 Hovan, S. A., and Rea, D.K., 1992, Paleocene Eocene boundary changes in atmospheric and

1167 oceanic circulation: A Southern Hemisphere record, Geology, v. 20, p. 15–18.

1168 doi.org/10.1130/00917613(1992)020<0015:PEBCIA>2.3.CO;2

1169

1170 Hovan, S.A., Rea, D.K., Pisias, N.G., 1991, Late Pleistocene Continental Climate and

1171 Oceanic Variability Recorded in Northwest Pacific Sediments, Paleoceanography and

1172 Paleoclimatology, v.6, p. 295-394.

1173 doi.org/10.1029/91PA00559

1174

1175 Hummel, G. and Kocurek, G., 1984, Interdune areas of the Back-Island dune field, North

1176 Padre-Island, Texas, Sedimentary Geology, v. 39, p. 1-26.

1177 doi.org/10.1016/0037-0738(84)90022-8

1178

1179 Hunter, R.E., 1977, Basic types of stratification in small eolian dunes, Sedimentology, v. 24,

1180 p. 361–387.

1181 doi.org/10.1111/j.1365-3091.1977.tb00128.x

1182

1183 Hunter, R.E., 1981, Stratification styles in eolian sandstones: Some Pennsylvanian to Jurassic

1184 examples from the western interior USA, in Ethridge, F.G. and Flore, R.M., eds., Recent and

1185 Ancient Non-Marine Depositional Environments, Models for Exploration, Society for

1186 Sedimentary Geology Special Publication, v. 31, p. 315-329.

1187 doi.org/10.2110/pec.81.31.0315

1188

1189   IPCC, 2007, Climate Change 2007: The Physical Science Basis, in Solomon, S., Qin, D.,

1190   Manning, M., Chen, Z., Marquis, M., Averyt, K.B., Tignor, M., and Miller, H.L., eds.,

1191   Contribution of Working Group I to the Fourth Assessment Report of the Intergovernmental

1192   Panel on Climate Change: Cambridge, Cambridge University Press, 996 p.

1193

1194   Irmen, A.P. and Vondra, C.F., 2000, Aeolian sediments in lower to middle (?) Triassic rocks

1195   of central Wyoming, Sedimentary Geology, v. 132, p. 69-88.

1196   doi.org/10.1016/S0037-0738(99)00129-3

1197

1198   Jones, L.S. and Blakey, R.C., 1997, Eolian-fluvial interaction in the Page Sandstone (Middle

1199   Jurassic) in south-central Utah, USA: A case study of erg-margin processes, Sedimentary

1200   Geology, v. 109, p. 181-198.

1201   doi.org/10.1016/S0037-0738(96)00044-9

1202

1203   Jones, F.H., dos Santos Scherer, C.M. and Kuchle, J., 2015, Facies architecture and

1204   stratigraphic evolution of aeolain dune and interdune deposits, Permian Caldeirao Member

1205   (Santa Brigida Formation), Brazil, Sedimentary Geology, v. 337, p. 133-150.

1206   doi.org/10.1016/j.sedgeo.2016.03.018

1207

1208   Jordan, O.D. and Mountney, N.P., 2010, Styles of interaction between aeolian, fluvial and

1209   shallow marine environments in the Pennsylvanian to Permian lower Cutler beds, south-east

1210   Utah, USA, Sedimentology, v. 57, p. 1357-1385.

1211   doi.org/10.1111/j.1365-3091.2010.01148.x

1212

1213   Jordan, O.D. and Mountney, N.P., 2012, Sequence stratigraphic evolution and cyclicity of an

1214   ancient coastal desert system: the Pennsylvanian-Permian Lower Cutler Beds, Paradox Basin,

1215   Utah, U.S.A, Journal of Sedimentary Research, v. 82, p. 755–780.

1216   doi.org/10.2110/jsr.2012.54

1217

1218   Kidder, D.L. and Worsley, T.R., 2010, Phanerozoic Large Igneous Provinces (LIPs), HEATT

1219   (Haline Euxinic Acidic Thermal Transgression) episodes, and mass extinctions:

1220   Palaeogeography, Palaeoclimatology, Palaeoecology, v. 295, p. 162–191.

1221   doi:10.1016/j.palaeo.2010.05.036.

1222

1223   Kidder, D.L. and Worsley, T.R., A human-induced hothouse climate? The Geological Society

1224   of America, v. 22, p. 4-11.

1225   doi.org/10.1130/G131A.1.

1226

1227   Knoll, A.H., and Walter, M.R., 1992. Latest Proterozoic stratigraphy and Earth history,

1228   Nature, v. 356, p. 673–677.

1229   doi.org/10.1038/356673a0

1230

1231   Kocurek, G., 1991, Interpretation of ancient eolian sand dunes, Annual Review of Earth and

1232   Planetary Science, v. 19, p. 43-75.

1233   doi.org/10.1146/annurev.ea.19.050191.000355.

1234

1235   Kocurek, G., 1996, Desert aeolian systems, in Reading, H.G., eds., Sedimentary

1236   environments: processes, facies and stratigraphy, pp. 125-153, 3rd edition, Oxford:

1237   Blackwell.

1238

1239   Kocurek G., 1999, The aeolian rock record (Yes, Virginia, it exists but it really is rather

1240   special to create one), in Goudie, A.S., Livingstone, I., Stokes, S., eds., Aeolian

1241   Environments Sediments and Landforms, pp. 239-259, John Wiley and Sons Ltd, Chichester.

1242

1243   Kocurek, G., 1998, Aeolian System Response to External Forcing Factors - A Sequence

1244   Stratigraphic View of the Saharan Region, in Alsharan, A.S., Glennie, K.W. and Whittle,

1245   G.L., eds., Quaternary Deserts and Climatic Change, pp. 327-338. Balkema,

1246   Rotterdam/Brookfield

1247

1248   Kocurek, G. and Day, M., 2018, What is preserved in the aeolian rock record? A Jurassic

1249   Entrada Sandstone case study at the Utah–Arizona border, Sedimentology, v. 65, p. 1301-

1250   1321.

1251   doi.org/10.1111/sed.12422

1252

1253   Kocurek, G. and Dott, R.H., 1981, Distinctions and uses of stratification types in the

1254   interpretation of eolian sand, Journal of Sedimentary Petrology, v. 51, p. 579-595.

1255   doi.org/10.1306/212F7CE3-2B24-11D7-8648000102C1865D

1256

1257   Kocurek, G. and Fielder, G., 1982, Adhesion structures, Journal of Sedimentary Petrology, v.

1258   52, p. 1229-1241.

1259   doi.org/10.1306/212F8102-2B24-11D7-8648000102C1865D

1260

1261 Kocurek, G. and Havholm, K.G., 1993, Eolian sequence stratigraphy-a conceptual

1262 framework, in Weimer, P. and Posamentier, H., eds., Siliciclastic Sequence Stratigraphy,

1263 American Association of Petroleum Geologists Memoir, v. 58, p. 393-409.

1264 doi.org/10.1306/M58581C16

1265

1266 Kocurek, G. and Lancaster, N., 1999, Aeolian system sediment state: theory and Mojave

1267 Desert Kelso dune field example, Sedimentology, v. 46, p. 505-515.

1268 doi.org/10.1046/j.1365-3091.1999.00227.x

1269

1270 Kocurek, G., Lancaster, N., Carr, M. and Frank, A, 1999, Tertiary Tsondab Sandstone

1271 Formation: preliminary bedform reconstruction and comparison to modern Namib Sand Sea

1272 dunes, Journal of African Earth Sciences, v. 29, p. 629-642.

1273 doi.org/10.1016/S0899-5362(99)00120-7

1274

1275 Kocurek, G., Townsley, M., Yeh, E., Havholm, K. and Sweet, M.L., 1992, Dune and dune-

1276 field development on Padre Island, Texas, with implications for interdune deposition and

1277 water-table controlled accumulation, Journal of Sedimentary Petrology, v. 62, p. 622-635.

1278 doi.org/10.1306/D4267974-2B26-11D7-8648000102C1865D

1279

1280 Kocurek, G., Robinson, N.I. and Sharp, J.M.J., 2001, The response of the water table in

1281 coastal aeolian systems to changes in sea level, Sedimentary Geology, v. 139, p. 1-13.

1282 doi.org/10.1016/S0037-0738(00)00137-8

1283

1284 Kohfeld, K. E. and Harrison, S.P., 2001, DIRTMAP: The geological record of dust, Earth

1285 Science Reviews, v. 54, p. 81–114.

1286   doi.org/10.1016/S0012-8252(01)00042-3

1287

1288   Krapovickas, V., 2012, Deposits of the Santa Cruz Formation (late early Miocene):

1289   paleohydrologic and paleoclimatic significance, in Vizcaíno, S.F., Kay, R.F. and Bargo,

1290   M.S., eds., Early Miocene paleobiology in Patagonia: High-latitude paleocommunities of the

1291   Santa Cruz Formation, pp. 91–103, Cambridge, Cambridge University Press.

1292

1293   Krumbein, W.C., 1941, Measurement and geological significance of shape and roundness of

1294   sedimentary particles, Journal of Sedimentary Petrology, v. 11, p. 64-72.

1295

1296   Kutzbach, J.E. and R.G. Gallimore, 1989, Pangaean climates: Megamonsoons of the

1297   megacontinent, Journal of Geophysical Research, v. 94, p. 3341-3357.

1298   doi.org/10.1029/JD094iD03p03341

1299

1300   Lancaster, N., 1989, The Namib Sand Sea: Dune forms, processes and sediments, Taylor and

1301   Francis, 1989 Rotterdam: Balkema, p. 180.

1302   ISBN: 9061916976, 9789061916970

1303

1304   Lancaster, N., 1990, Palaeoclimatic evidence from sand seas, Palaeogeography,

1305   Palaeoclimalology, and Palaeoecology, v. 76, p. 279-90.

1306   doi.org/10.1016/0031-0182(90)90116-O

1307

1308   Lancaster, N. and Teller, J.T., 1988, Interdune deposits of Namib Sand Sea, Sedimentary

1309   Geology, v. 55, p. 91-107.

1310   doi.org/10.1016/0037-0738(88)90091-7

1311

1312 Lauretano, V., Littler, K., Polling, M., Zachos, J. C. and Lourens, L. J., 2015, Frequency,

1313 magnitude and character of hyperthermal events at the onset of the Early Eocene Climatic

1314 Optimum, Climate of the Past, v. 11, p. 1313–1324.

1315 doi.org/10.5194/cp-11-1313-2015.

1316

1317 Leleu, S. and Hartley, A.J., 2018, Constraints on synrift intrabasinal horst development from

1318 alluvial fan and aeolian deposits (Triassic, Fundy Basin, Nova Scotia), in Ventra, D. and

1319 Clarke, L.E., Geology and Geomorphology of Alluvial and Fluvial Fans: Terrestrial and

1320 Planetary Perspectives, Geological Society of London Special Publication, v. 440, p. 79-101.

1321 doi.org/10.1144/SP440.8

1322

1323 Liesa, C.L., Rodríguez-López, J.P., Ezquerro, L., Alfaro, P., Rodriguez-Pascua, M.A.,

1324 Lafuente, P., Arlegui, L. and Simon J.L., 2016, Facies control on seismites in an alluvial-

1325 aeolian system: The Pliocene dunefield of the Teruel half-graben basin (eastern Spain),

1326 Sedimentary Geology, v. 344, p. 237-252.

1327 doi.org/10.1016/j.sedgeo.2016.05.009

1328

1329 Link P.K., 2009, "Icehouse" (Cold) Climates, in Gornitz V., eds., Encyclopedia of

1330 Paleoclimatology and Ancient Environments. Encyclopedia of Earth Sciences Series.

1331 Springer, Dordrecht.

1332 doi.org/10.1007/978-1-4020-4411-3_112

1333

1334 Long, D.G.F., 2006, Architecture of pre-vegetation sandy-braided perennial and Ephemeral

1335 River deposits in the Paleoproterozoic Athabasca Group, northern Saskatchewan, Canada as

1336 indicators of Precambrian fluvial style, Sedimentary Geology, v. 190, p. 71-95.

1337 doi.org/10.1016/j.sedgeo.2006.05.006

1338

1339 Loope, D.B., 1985, Episodic deposition and preservation of eolian sands – a Late Paleozoic

1340 example from southeastern Utah, Geology, v. 13, p. 73– 76.

1341 doi.org/10.1130/0091-7613(1985)13<73:EDAPOE>2.0.CO;2

1342

1343 Loope, D.B. and Rowe C.M., 2003, Long-lived pluvial episodes during deposition of the

1344 Navajo Sandstone, The Journal of Geology, v. 111, p. 223-232.

1345 doi.org/10.1086/345843

1346

1347 Loope, D., Rowe, C. and Joeckel, R., 2001, Annual monsoon rains recorded by Jurassic

1348 dunes, Nature, v. 412, p. 64–66.

1349 doi.org/10.1038/35083554

1350

1351 Loope, D.B., Swinehart, J.B. and Mason, J.P., 1995, Dune-dammed paleovalleys of the

1352 Nebraska Sand Hills- intrinsic versus climatic controls on the accumulation of lake and marsh

1353 sediments, The Geological Society of America Bulletin, v. 107, p. 396-406.

1354 doi.org/10.1130/0016-7606(1995)107<0396:DDPOTN>2.3.CO;2

1355

1356 Lu, J., Vecchi, G. A., and Reichler, T., 2007, Expansion of the Hadley cell under global

1357 warming, Geophysical Research Letters, v. 34, L06805.

1358 doi.org/10.1029/2006GL028443

1359

1360 Mainguet, M. and Chemin, M. C., 1983, Sand seas of the Sahara and Sahel: an explanation of

1361 their thickness and sand dune type by the sand budget principle, in Brookfield, M.E. and

1362 Ahlbrandt, T.S., eds., Eolian Sediments and Processes, Developments in Sedimentology, v.

1363 38, p. 353-363.

1364 doi.org/10.1016/S0070-4571(08)70804-5

1365

1366 McElhinny, M., Embleton, B.J.J., Ma, X.H. and Zhang, Z.K., 1981, Fragmentation of Asia in

1367 the Permian, Nature, v. 293, p. 212-216.

1368 doi.org/10.1038/293212a0

1369

1370 Meadows, N.S. and Beach, A., 1993, Structural and climatic controls on facies distribution in

1371 a mixed fluvial and aeolian reservoir: the Triassic Sherwood Sandstone in the Irish Sea, in

1372 North, C.P. and Prosser, D.J., eds., Characterization of fluvial and aeolian reservoirs,

1373 Geological Society of London Special Publication, v. 73, p. 247-264.

1374 doi.org/10.1144/GSL.SP.1993.073.01.15

1375

1376 Melton M.A., 1965, The geomorphic and paleoclimatic significance of alluvial deposits in

1377 southern Arizona, The Journal of Geology, v. 73, p. 1–38.

1378 doi.org/10.1086/627044

1379

1380 Middleton, G.V. and Southard, J.B., 1984, Mechanics of Sediment Movement, Society for

1381 Sedimentary Geology Short Course, 3, 401 pp.

1382

1383 Milankovitch, M., 1941, Kanon der Erdbestrahlung und seine Andwendung auf das

1384 Eiszeiten-problem, Royal Serbian Academy, Belgrade.

1385

1386 Mitchum, R. M., 1977, Seismic stratigraphy and global changes of sea level, Part I: Glossary

1387 of terms used in seismic stratigraphy, in Payten, C. E., ed., Seismic stratigraphy--applications

1388 to hydrocarbon exploration American Association of Petroleum Geologists Memoir, v. 26, p.

1389 53-62.

1390 doi.org/10.1306/M26490C13

1391

1392 Montañez, I.P. and Poulsen, C.J., 2013, The Late Paleozoic Ice Age: An Evolving Paradigm,

1393 Annual Review of Earth and Planetary Science, v. 41, p. 629-656.

1394 doi.org/10.1146/annurev.earth.031208.100118

1395

1396 Morley, C.K., 1995, Developments in the structural geology of rifts over the last decade and

1397 their impact on hydrocarbon exploration, in Lambiase, J.J., ed., Hydrocarbon Habitat in Rift

1398 Basins, Geological Society of London, Special Publication 80, p. 1–32.

1399 doi.org/10.1144/GSL.SP.1995.080.01.01

1400

1401 Mountney, N.P., 2006, Periodic accumulation and destruction of aeolian erg sequences: The

1402 Cedar Mesa Sandstone, White Canyon, southern Utah, Sedimentology, v. 53, p. 789-823.

1403 doi.org/10.1111/j.1365-3091.2009.01072.x

1404

1405 Mountney, N.P. and Howell, J., 2000, Aeolian architecture, bedform climbing and

1406 preservation space in the Cretaceous Etjo Formation, NW Nambia, Sedimentology, v. 47, p.

1407 825-849.

1408   doi.org/10.1046/j.1365-3091.2000.00318.x

1409

1410   Mountney, N.P. and Jagger, A., 2004, Stratigraphic evolution of an aeolian erg margin

1411   system: the Permian Cedar Mesa Sandstone, SE Utah, USA, Sedimentology, v. 51, p. 713-

1412   743.

1413   doi.org/10.1111/j.1365-3091.2004.00646.x

1414

1415   Mountney, N.P. and Russell, A.J., 2006, Coastal aeolian dune development, Solheimasandur,

1416   southern Iceland, Sedimentary Geology, v. 192, p. 167-181.

1417   doi.org/10.1016/j.sedgeo.2006.04.004

1418

1419   Mountney, N.P. and Russell, A.J., 2009, Aeolian dune-field development in a water-table

1420   controlled system: Skiđeararsándur, Southern Iceland, Sedimentology, v. 56, p. 2107-2131.

1421   doi.org/10.1111/j.1365-3091.2009.01072.x

1422

1423   Mountney, N.P., Howell, J., Flint, S. and Jerram, D., 1999, Climate, sediment supply and

1424   tectonics as controls on the deposition and preservation of the aeolian-fluvial Etjo Sandstone

1425   Formation, Namibia, Journal of the Geological Society of London, v. 156, p. 771-777.

1426   doi.org/10.1144/gsjgs.156.4.0771

1427

1428   Newell, A.J., 2001, Bounding surfaces in a mixed aeolian-fluvial system (Rotliegend,

1429   Wessex Basin, SW UK), Marine and Petroleum Geology, v. 18, p. 339-347.

1430   doi.org/10.1016/S0264-8172(00)00066-0

1431

1432 Nielson J. and Kocurek G., 1986, Climbing zibars of the Algodones, Sedimentary Geology,

1433 v. 48, p. 1-15.

1434 doi.org/10.1016/0037-0738(86)90078-3

1435

1436 Nielsen, K.A., Clemmensen, L.B. and Fornós, J.J., 2004, Middle Pleistocene

1437 magnetostratigraphy and susceptibility stratigraphy: data from a carbonate Aeolian system,

1438 Mallorca, Western Mediterranean. Quaternary Science Reviews, v. 23, p. 1733–1756.

1439 doi.org/10.1016/j.quascirev.2004.02.006

1440

1441 Nichols, G.J., 2005, Sedimentary evolution of the lower Clair Group, Devonian, west of

1442 Shetland; climate and sediment supply controls on fluvial, aeolian and lacustrine deposition,

1443 in Doré, A.G. and Vining, B.A., eds., Petroleum Geology of Northwest Europe, Proceedings

1444 of the Conference, published by the Geological Society of London, v. 6, p. 957-967.

1445 doi.org/10.1144/0060957

1446

1447 Nickling, W.G., McKenna Neuman, C. and Lancaster, N., 2002, Grainfall processes in the lee

1448 of transverse dunes, Silver Peak, Nevada, Sedimentology, v. 49, p. 191–209.

1449 doi.org/10.1046/j.1365-3091.2002.00443.x

1450

1451 Olsen, H., Due, P.H. and Clemmensen, L.B., 1989, Morphology and genesis of asymmetric

1452 adhesion warts—a new adhesion surface structure, Sedimentary Geology, v. 61, p. 277-285.

1453 doi.org/10.1016/0037-0738(89)90062-6

1454

1455 Parrish, J.T., 1993, Climate of the supercontinent Pangea, The Journal of Geology, v. 101, p.

1456 215–233.

1457   doi.org/10.1086/648217

1458

1459   Parrish, J.T. and Petersen, F., 1988, Wind directions predicted from global circulation models

1460   and wind directions determined from eolian sandstones of the western United States- A

1461   comparison, Sedimentary Geology, v. 56, p. 261-282.

1462   doi.org/10.1016/0037-0738(88)90056-5

1463

1464   Peters, G.P., Andrew, R.M., Canadell, J.G., Friedlingstein, P., Jackson, R.B., Korsbakken,

1465   J.I., Le Quéré, C. and Peregon, A., 2020, Carbon dioxide emissions continue to grow amidst

1466   slowly emerging climate policies, Nature Climate Change, v. 10, p. 3–6.

1467   doi.org/10.1038/s41558-019-0659-6

1468

1469   Peterson, F., 1988, Pennsylvanian to Jurassic eolian transportation systems in the western

1470   United States, in G. Kocurek, G., ed., Late Palaeozoic and Mesozoic Eolian Deposits of the

1471   Western Interior of the United States, Sedimentary Geology, v. 56, p. 207-260.

1472   doi.org/10.1016/0037-0738(88)90055-3

1473

1474   Petit, J.R., Jouzel, J., Raynaud, D., Barkov, N.I., Barnola, J.-M., Basile, I., Bender, M.,

1475   Chappellaz, J., Davis, M., Delaygue, G., Delmotte, M., Kotlyakov, V.M., Legrand, M.,

1476   Lipenkov, V.Y., Lorius, C., Pépin, L., Ritz, C., Saltzman, E., and Stievenard, M., 1999,

1477   Climate and atmospheric history of the past 420,000 years from the Vostok ice core,

1478   Antarctica, Nature, v. 399, p. 429–436.

1479   doi.org/10.1038/20859

1480

1481   Pike, J.D. and Sweet, D.E., 2018, Environmental drivers of cyclicity recorded in lower

1482   Permian eolian strata, Manitou Springs, western United States, Palaeogeography,

1483   Palaeoclimatology, Palaeoecology, v. 499, p. 1-12.

1484   doi.org/10.1016/j.palaeo.2018.03.026

1485

1486   Plint, G., Nummedal, D., 2000, The falling stage systems tract: Recognition and importance

1487   in sequence stratigraphic analysis, Geological Society London Special Publications, v. 172, p.

1488   1-17.

1489   doi.org/10.1144/GSL.SP.2000.172.01.01.

1490

1491   Porter, M.L., 1986, Sedimentary record of erg migrations, Geology, v. 14, p. 497-500.

1492   doi.org/10.1130/0091-7613(1986)14<497:SROEM>2.0.CO;2

1493

1494   Price, G., Valdes, P.J and Sellwood, B.W., 1998, A comparison of GCM simulated

1495   Cretaceous 'greenhouse' and 'icehouse' climates: implications for the sedimentary record,

1496   Palaeogeography, Palaeoclimatology, Palaeoecology, v. 142, p. 123–138.

1497   doi.org/10.1016/S0031-0182(98)00061-3

1498

1499   Pulvertaft, T.C.R., 1985, Eolian dune and wet interdune sedimentation in the Middle

1500   Proterozoic Dala Sandstone, Sweden, Sedimentary Geology, v. 44, p. 93-111.

1501   doi.org/10.1016/0037-0738(85)90034-X

1502   Purser, B.H. and Evans, G., 1973, Regional sedimentation along the Trucial Coast, Persian

1503   Gulf, in Purser, B.H., eds., Persian Gulf, p.211-231, Berlin, Springer.

1504

1505 Pye, K., 1983, Early Post-Depositional Modification of Aeolian Dune Sands, in Brookfield,

1506 M.E. and Ahlbrandt, T.S., eds., Developments in Sedimentology, v. 38, p. 197-221.

1507 doi.org/10.1016/S0070-4571(08)70796-9.

1508

1509 Pye, K., 2009, Aeolian bed forms, in Pye, K. and Tsoar, H., Aeolian sand and sand dunes,

1510 Unwin Hyman Limited, London, p. 175-253.

1511 ISBN : 978-3-540-85909-3

1512

1513 Pye, K. and Tsoar, H., 1990, Aeolian sand and sand dunes, Unwin Hyman Limited, London,

1514 pp. 396.

1515 ISBN : 978-3-540-85909-3

1516

1517 Rainbird, R.H., 1992, Anatomy of a large-scale braid-plain quartzarenite from the

1518 Neoproterozoic Shaler Group, Victoria Island, Northwest Territories, Canada, Canadian

1519 Journal of Earth Science, v. 29, p. 2537-2550.

1520 doi.org/10.1139/e92-201

1521

1522 Rea, D. K., 1994, The paleoclimatic record provided by eolian deposition in the deep sea:

1523 The geologic history of wind, Reviews of Geophysics, v. 32, p. 159–195.

1524 doi.org/10.1029/93RG03257.

1525

1526 Rea, D.K., Janecek, T.R., 1981, Mass-accumulation rates of the non-authigenic inorganic

1527 crystalline (Eolian) component of deep-sea sediments from the western Mid-Pacific

1528 Mountains, Deep Sea Drilling Project Site 463, in Thiede, J., Vallier, T.L., et al., eds., Initial

1529 Reports of the Deep Sea Drilling Project (U.S. Govt. Printing Office), v. 62, p. 653-659.

1530

1531 Reis, A.D.d., Scherer, C.M.S., Amarante, F.B., Rossetti, M.M.M., Kifumbi, C., Souza, E.G.,

1532 Formolo Ferronatto, J.P and Owen, A., 2020, Sedimentology of the proximal portion of a

1533 large-scale, Upper Jurassic fluvial-aeolian system in Paraná Basin, southwestern Gondwana.

1534 Journal of South American Earth Sciences, v. 95, 102248.

1535 doi.org/10.1016/j.jsames.2019.102248

1536

1537 Rodríguez-López, J.P., Meléndez, N., de Boer, P.L. and Soria, A.R. , 2012, Controls on

1538 marine-erg margin cycle variability: aeolian-marine interaction in the Mid-Cretaceous Iberian

1539 Desert System, Spain, Sedimentology, v. 59, p. 466-501.

1540 doi.org/10.1111/j.1365-3091.2011.01261.x

1541

1542 Rodríguez-López, J.P., Clemmensen, L.B., Lancaster, N., Mountney, N.P. and Veiga, G.D.,

1543 2014, Archean to Recent aeolian sand systems and their sedimentary record: Current

1544 understanding and future prospects, Sedimentology, v. 61, p. 1487-1534.

1545 doi.org/10.1111/sed.12123

1546

1547 Rosendahl, B.R., 1987, Architecture of continental rifts with special reference to East Africa,

1548 Annual Review of Earth and Planetary Sciences, v. 15, p. 445–503.

1549 doi.org/10.1146/annurev.ea.15.050187.002305

1550

1551 Rowley, D.B., Raymond, A., Parrish, J.T., Lottes, A.L., Scotese, C.R. and Ziegler, A.M.,

1552 1985, Carboniferous paleogeographic, phytogeographic, and paleoclimatic reconstructions,

1553 International Journal of Coal Geology, v. 5, p. 7–42. doi.org/10.1016/0166-5162(85)90009-6

1554

1555 Rubin, D.M. and Hunter, R.E., 1982, Bedform climbing in theory and nature, Sedimentology,

1556 v. 29, p. 121– 138.

1557 doi.org/10.1111/j.1365-3091.1982.tb01714.x

1558

1559 Ruz, M.-H. and Allard, M., 1994, Coastal dune development in cold-climate environments,

1560 Physical Geography, v. 15, p. 372–380.

1561 doi.org/10.1080/02723646.1994.10642523

1562 Sadler, P.M., 1981, Sediment accumulation rates and the completeness of stratigraphic

1563 sections, The Journal of Geology, v. 89, p. 569–584.

1564 doi.org/10.1086/628623

1565

1566 Sames, B., Wagreich, M., Conrad, C.P. and Iqbal, S., 2020, Aquifer-eustasy as the main

1567 driver of short-term sea-level fluctuations during Cretaceous hothouse climate phases,

1568 Geological Society of London Special Publications, 498, p. 9-38.

1569 doi.org/10.1144/SP498-2019-105

1570

1571 Sarnthein, M., 1978, Sand deserts during glacial maximum and climatic optimum, Nature, v.

1572 272, p. 43-46.

1573 doi.org/10.1038/272043a0

1574

1575 Scherer, M.S., Lavina, E.L.C., Dias Filho, D.C., Oliveira, F.M., Bongiolo, D.E. and Aguiar,

1576 E.S., 2007, Stratigraphy and facies architecture of the fluvial-aeolian-lacustrine Sergi

1577 Formation (Upper Jurassic), Reconcavo Basin, Brazil, Sedimentary Geology, v. 194, p. 169-

1578 193.

1579 doi.org/10.1016/j.sedgeo.2006.06.002

1580

1581   Scherer, C.M.S. and Goldberg, K., 2007, Palaeowind patterns during the latest Jurassic-

1582   earliest Cretaceous in Gondwana: Evidence from aeolian cross-strata of the Botucatu

1583   Formation, Brazil, Palaeogeography, Palaeoclimatology, Palaeoecology, v. 250, p. 89-100.

1584   doi.org/10.1016/j.palaeo.2007.02.018.

1585

1586   Scherer, C.M.A. and Lavina, L.C., 2005, Sedimentary cycles and facies architecture of

1587   aeolian–fluvial strata of the Upper Jurassic Guara Formation, southern Brazil,

1588   Sedimentology, v. 52, p. 1323-1341.

1589   doi.org/10.1111/j.1365-3091.2005.00746.x

1590

1591   Scherer, C.M.S., Mello, R.G., Ferronatto, J.P.F, Amarante, F.B., Reis, A.D., Souza, E.G., and

1592   Goldberg, K,, 2020, Changes in prevailing surface-palaeowinds of western Gondwana

1593   during Early Cretaceous, Cretaceous Research, v. 116, 104598

1594

1595   Schlische, R.W., 1993, Anatomy and evolution of the Triassic-Jurassic continental rift

1596   system, eastern North America, Tectonics, v. 12, p. 1026–1042.

1597   doi.org/10.1029/93TC01062

1598

1599   Schokker, J. and Koster, E.A., 2004, Sedimentology and facies distribution of Pleistocene

1600   cold-climate aeolian and fluvial deposits in the Roer Valley graben (Southeastern

1601   Netherlands), Permafrost and Periglacial Processes, v. 15, p. 1-20.

1602   doi.org/10.1002/ppp.477

1603

1604 Semeniuk, V. and Glassford D.K., 1988, Significance of aeolian limestone lenses in quartz

1605 sand formations: an interdigitation of coastal and continental facies, Perth Basin,

1606 southwestern, Australia, Sedimentary Geology, v. 57, p. 199-209.

1607 doi.org/10.1016/0037-0738(88)90027-9

1608

1609 Shackleton, N.J., Crowhurst, S.J., Weedon, G., and Laskar, L., 1999, Astronomical

1610 calibration of Oligocene-Miocene time: Royal Society of London Philosophical Transactions,

1611 v. 357, p. 1909–1927.

1612 doi.org/10.1098/rsta.1999.0407

1613

1614 Shaw, R.D., Etheridge, M.A. and Lambeck, K., 1991, Development of the Late Proterozoic to

1615 Mid-Paleozoic, intracratonic Amadeus Basin in central Australia: A key to understanding

1616 tectonic forces in plate interiors, Tectonics, v. 10, p. 688-721.

1617 doi.org/10.1029/90TC02417

1618

1619 Simplicio, F. and Basilici, G., 2015, Unusual thick eolian sand sheet sedimentary succession:

1620 Paleoproterozoic Bandeirinha Formation, Minas Gerais, Brazilian Journal of Geology, v. 45,

1621 p. 3-11.

1622 doi.org/10.1590/2317-4889201530133

1623

1624 Simpson, E.L., Eriksson, K.A. and Muller, W.U., 2012, 3.2 Ga eolian deposits from the

1625 Moodies Group, Barberton Greenstone Belt, South Africa: Implications for the origin of first-

1626 cycle quartz sandstones, Precambrian Research, v. 214-215, p. 185-191.

1627 doi.org/10.1016/j.precamres.2012.01.019

1628

1629 Simpson, E.L., Fernando, A., Pradip, B., Bumby, A.J., Eriksson, K.A., Eriksson, P.G.,

1630 Martins-Neto, M.A., Middleton, L.T. and Rainbird, R., 2004, Sedimentary dynamics in

1631 Precambrian aeolianites. In Eriksson, P.G., Altermann, W., Nelson, D.R., Mueller, W. and

1632 Catuneanu, O., eds., The Precambrian Earth: Tempos and Events, Elsevier, Amsterdam,

1633 pp. 675-677.

1634

1635 Simpson, E.L., Heness, E., Bumby, A., Eriksson, P.G., Eriksson, K.A., Hilbert-Wolf, H.L.,

1636 Linnevelt, S., Fitzgerald Malena, H., Modungwa, T. and Okafor, O.J., 2013, Evidence for

1637 2.0Ga continental microbial mats in a paleodesert setting. Precambrian Research, v. 237, p.

1638 36-50.

1639 doi.org/10.1016/j.precamres.2013.08.001.

1640

1641 Simpson, E.L., Hilbert-Wolf, H.L., Simpson, W.S., Tindall, S.E., Bernard, J.J., Jenesky, T.A.

1642 and Wizevich, M.C., 2008, The interaction of aeolian and fluvial processes during deposition

1643 of the Upper Cretaceous capping sandstone member, Wahweap Formation, Kaiparowits

1644 Basin, Utah, U.S.A. Palaeogeography, Palaeoclimatology, Palaeoecology, v. 270, p. 19-28.

1645 doi.org/10.1016/j.palaeo.2008.08.009.

1646

1647 Smith, A.G., Briden, J.C. and Drewry, G.E., 1973, Phanerozoic world maps, in Hughes, N.F.,

1648 ed., Organisms and Continents through Time, Special Paper of the Paleontological

1649 Association 12, p. 1-42.

1650

1651 Sorby, H.C., 1859, On the structures produced by the currents present during the deposition

1652 of stratified rocks, The Geologist, v. 2, p. 137–147.

1653 doi.org/10.1017/S1359465600021122

1654

1655 Soreghan, G.S., Heavens, N.G., Hinnov, L.A., Aciego, S.M., Simpson, C., 2015,

1656 Reconstructing the Dust Cycle in Deep Time: the Case of the Late Paleozoic Icehouse, The

1657 Paleontological Society Papers, v. 21, p. 83-120.

1658 doi.org/10.1017/S1089332600002977.

1659

1660 Soria, A.R., Liesa, C.L., Rodríguez-López, J.P., Meléndez, N., de Boer, P.L. and Meléndez,

1661 A., 2011, An Early Triassic evolving erg system (Iberian Chain, NE Spain): Palaeoclimate

1662 implications, Terra Nova, v. 23, p. 76-84.

1663 doi.org/10.1111/j.1365-3121.2011.00986.x

1664

1665 Stancin, A.M., Gleason, J.D., Hovan, S.A., Rea, D.K., Owen, R.M., More, T.C. Jr., Hall,

1666 C.M. and Blum, J.D., 2008, Miocene to recent eolian dust record from the southwest Pacific

1667 Ocean at 40°S latitude, Palaeogeography, Palaeoclimatology, Palaeoecology, v. 261, p. 218–

1668 233.

1669 doi.org/10.1016/j.palaeo.2007.12.015

1670

1671 Stewart, J.H., 2005, Eolian deposits in the Neoproterozoic Big Bear Group, San Bernardino

1672 Mountains, California, USA, Earth Science Reviews, v. 72, p. 47-62.

1673 doi.org/10.1016/j.earscirev.2005.07.012

1674

1675 Strömbäck, A. and Howell, J.A., 2002, Predicting distribution of remobilized aeolian facies

1676 using sub-surface data: the Weissliegend of the UK Southern North Sea, Petroleum

1677 Geoscience, v. 8, p. 237–249.

1678 doi.org/10.1144/petgeo.8.3.237

1679

1680   Stokes, W.L., 1968, Multiple parallel-truncation bedding planes – a feature of wind deposited

1681   sandstone formations, Journal of Sedimentary Petrology, v. 38, p. 510–515.

1682   doi.org/10.1306/74D719D3-2B21-11D7-8648000102C1865D

1683

1684   Taylor, I.E. and Middleton, G.V., 1990, Aeolian sandstone in the Copper Harbor Formation,

1685   Late Proterozoic, Lake Superior basin, Canadian Journal of Earth Science, v. 27, p. 1339-

1686   1347.

1687   doi.org/10.1139/e90-144

1688

1689   Trewin, N.H., 1993, Controls on fluvial deposition in mixed fluvial and aeolian facies within

1690   the Tumblagooda Sandstone (Late Silurian) of Western-Australia, Sedimentary Geology, v.

1691   85, p. 387–400.

1692   doi.org/10.1016/0037-0738(93)90094-L

1693

1694   Van Wagoner, J.C., Mitchum, R.M., Campion, K.M. and Rahmanian, V.D., 1990,

1695   Siliciclastic Sequence Stratigraphy in Well Logs, Cores, and Outcrops: Concepts for High-

1696   Resolution Correlation of Time and Facies, Tulsa, Oklahoma, American Association for

1697   Petroleum Geologists Methods in Exploration Series v. 7, p. 1-55.

1698   doi.org/10.1306/Mth7510

1699

1700   Vanden Berg, M. D. and Jarrard, R.D., 2004, Cenozoic mass accumulation rates in the

1701   equatorial Pacific based on high-resolution mineralogy of Ocean Drilling Program Leg 199,

1702   Paleoceanography, 19, PA2021.

1703   doi.org/10.1029/2003PA000928

1704

1705 Veiga, G.D., Spalletti, L.A. and Flint, S.S., 2002, Aeolian/fluvial interactions and high-

1706 resolution sequence stratigraphy of a non-marine lowstand wedge: the Avile Member of the

1707 Agrio Formation (Lower Cretaceous), central Neuquen Basin, Argentina, Sedimentology, v.

1708 49, p. 1001-1019.

1709 doi.org/10.1046/j.1365-3091.2002.00487.x

1710

1711 Voss, R., 2002, Cenozoic stratigraphy of the southern Salar de Antofalla region, northwestern

1712 Argentina, Revista geológica de Chile, v. 29, p. 167-189.

1713 doi.org/10.4067/S0716-02082002000200002

1714

1715 Wanless, H.R. and Shepard, F.P., 1936, Sea level and climatic changes related to late

1716 Paleozoic cycles, Geological Society of America Bulletin, v. 47, p. 1177–1206.

1717 doi.org/10.1130/GSAB-47-1177

1718

1719 West, R.R., Archer, A.W. and Miller, K.B., 1997, The role of climate in stratigraphic patterns

1720 exhibited by Late Paleozoic rocks exposed in Kansas, Palaeogeography, Palaeoclimatology,

1721 Palaeoecology, v. 128, p. 1–16.

1722 doi.org/10.1016/S0031-0182(97)81127-3

1723

1724 Westerhold, T., Röhl, U., Donner, B., McCarren, H. K. and Zachos, J. C., 2011, A complete

1725 high-resolution Paleocene benthic stable isotope record for the central Pacific (ODP Site

1726 1209), Global Biogeochemistry, v. 25, p. 1–13.

1727 doi.org/10.1029/2010PA002092

1728

1729   Wilson, I. G., 1971, Desert sandflow basins and a model for the development of ergs. The

1730   Geographical Journal, v. 137, p. 180-199.

1731   doi.org/10.2307/1796738

1732

1733   Wilson, I. G., 1973, Ergs, Sedimentary Geology, v. 10, p. 77-106.

1734   doi.org/10.1016/0037-0738(73)90001-8

1735

1736   Winckler, G., Anderson, R.F., Fleisher, M.Q., McGee, D., and Mahowald, N., 2008,

1737   Covariant glacial-interglacial dust fluxes in the equatorial Pacific and Antarctica, Science, v.

1738   320, p. 93–96.

1739   doi.org/10.1126/science.1150595.

1740

1741   Withjack, M.O., Schlische R.W., Olsen P.E., 2002, Rift-basin structure and its influence on

1742   sedimentary systems, in Renaut, R.W. and Ashley G.M., ed., Sedimentation in Continental

1743   Rifts, Society for Sedimentary Geology, Special Publication 73.

1744   doi.org/10.2110/pec.02.73

1745

1746   Woodard, S.C., Thomas, D.J., Hovan, S., Röhl, U. and Westerhold, T., 2011, Evidence for

1747   orbital forcing of dust accumulation during the early Paleogene greenhouse, Geochemistry,

1748   Geophysics, Geosystems, v. 12, Q02007.

1749   doi.org/10.1029/2010GC003394

1750

1751   Zavala, C. and Freije, R.H., 2001, On the understanding of aeolian sequence stratigraphy: An

1752   example from Miocene-Pliocene deposits in Patagonia, Argentina, Rivista Italiana di

1753   Paleontologia e Stratigrafia, v. 107, p. 251-264.

1754   doi.org/10.13130/2039-4942/5435

1755

1756   Ziegler, A.M., Scotese, C.R. and Barrett, S.F., 1983, Mesozoic and Cenozoic

1757   paleogeographic maps, in Brosche, P. and Sundermann, J., eds., Tidal friction and the earth's

1758   rotation. II: Springer, Verlag, Berlin, p. 240-252.

1759   doi.org/10.1007/978-3-642-68836-2_17

1760

1761   **FIGURE CAPTIONS**

1762

1763   1.   A) Distribution of case studies used in this investigation, coloured according to icehouse

1764   (blue) and greenhouse (orange) conditions (this colour scheme applies throughout this

1765   account). The shape of the marker indicates the paleosupercontinental setting of the case

1766   study. B) Geological time-scale showing the five major icehouse periods (labelled A-E)

1767   and the distribution of the supercontinents. For all icehouse case-studies, the marker

1768   contains a letter (A-E) denoting the associated icehouse period.

1769   2.   Factors commonly associated with icehouse and greenhouse conditions. Boxes A-E are

1770   theoretical. F) Low latitude sea surface temperatures (based on estimates in Forster et al.,

1771   2007). G) Estimates of pCO2 (based on values in Shaviv and Veizer, 2003). H) Pole to

1772   equator thermal contrast. I) Planetary windbelt speed (V = velocity). J) Wind shear (V^2=

1773   wind velocity squared). K) Wind erosive power (V^3= wind velocity cubed). Boxes H-K

1774   are based on the estimates of Kidder and Worsley (2010); the units for boxes I-K are

1775   expressed as fractions of the maximum (e.g., 0.67 would be 2/3 of the maximum). Figure

1776   adapted in part from Kidder and Worsley (2012).

1777   3.   Percentages of: A) eolian and non-eolian architectural elements, B) dune set, sandsheet

1778   and interdune elements, and C) non-aeolian elements, deposited under icehouse and

1779   greenhouse conditions. Percentages of eolian and non-eolian architectural elements are

1780   determined based on total element counts. For descriptions of eolian and non-eolian

1781   architectural element types see Table 2.

1782 4. Box and whisker plots showing distributions in element thickness for icehouse and

1783   greenhouse conditions: A) all eolian elements; B) dune sets; C) sandsheets; D) interdunes;

1784   E) all eolian facies. For descriptions of eolian architectural element types see Table 2.

1785 5. Percentages of: A) wet, dry, and damp interdunes; and the distribution of facies in B)

1786   interdunes and C) sandsheets. The percentages are determined based on the total element

1787   count. For descriptions of interdune types and facies element types see Table 2.

1788 6. Box and whisker plots of icehouse and greenhouse textural properties. A) modal grain-

1789   size; B) sorting; C) grain roundness.

1790 7. Percentages of supersurface descriptions. A) Bypass and deflation surfaces; B) surface

1791   'wetness'; C) surface stabilization. Percentages are calculated based on numbers of

1792   occurrences in vertical sections. For full descriptions of surface types and associated

1793   attributes see Table 2.

1794 8. Box and whisker plots of element thickness for elements grouped by: A) Proterozoic and

1795   Pangean paleosupercontinental settings; B) rift, foreland and intracratonic basin settings;

1796   for descriptions of basin types see Table 2; C) different paleolatitudes; and D) different

1797   dune-field physiographic settings.

1798 9. Scatterplot showing values of icehouse and greenhouse eolian element thicknesses for

1799   different paleolatitudes with mean and median overlain.

1800 10. Cycles of eolian accumulation and deflation under icehouse glacials and interglacials with

1801   accompanying sequence stratigraphic terminology. A) Deposition of thin sandsheet and

1802   dune-set elements associated with the onset of glacial conditions. B) Deposition of thick

1803   dune sets associated with strong trade-wind strengths and high rates of sediment supply in

1804   an arid setting. Both A and B show a relative fall in the level of the water table. C) Onset

1805   of deflation as a sediment source is exhausted. D) As interglacial conditions proceed,

1806   deflation continues to the level of the water table. Both C and D show a rise in the relative

1807   level of the water table, associated with more humid interglacial conditions. The rise in

1808   the level of the water table protects the lower part of the aeolian succession from erosion.

1809   E-G the start of a new glacial/interglacial cycle. The indicative lateral and vertical scales

1810   in Part A apply to all box models.

1811 11. Deposition of an eolian sequence under greenhouse conditions. The temporal sediment

1812   supply remains relatively static (A-D). An elevated water table associated with relatively

1813   humid conditions promotes the preservation of eolian dune sets by protecting them from

1814   potential wind erosion; accumulated dune sets are sequestered into the geological record

1815   (B-D). The generation of supersurfaces is most likely to be associated with fluvial

1816   inundation or due to a transition from eolian to sabkha deposition (C). The indicative

1817   lateral and vertical scales in Part A apply to all box models.

1818 12. Percentages of different basin-setting types (continental rift, foreland and intracratonic)

1819   for Proterozoic age case studies, subdivided into icehouse and greenhouse conditions.

1820 13. Box and whisker plots showing eolian architectural element thicknesses for Proterozoic,

1821   Pangean and Gondwanaland paleosupercontinenal settings.

1822

1823 **TABLE CAPTIONS**

1824

1825 1. List of the case studies used in this investigation. The geographic location of each case

1826   study is outlined in Figure 1 (identified via the case number). The reference refers to the

1827   original source material from which quantitative metrics were derived.

1828   2. Definitions of eolian and non-eolian architectural element types, facies element types,

1829   surface types, and basin types discussed in the text.

1830   3. Results of statistical analysis; SD: standard deviation; $P(T<=t)$: one tail t-test; ANOVA:

1831   analysis of variance. All results are reported to two decimal places, where appropriate.

1832   For all statistical calculations see Supplementary Information.

1833

1834

Figure 1
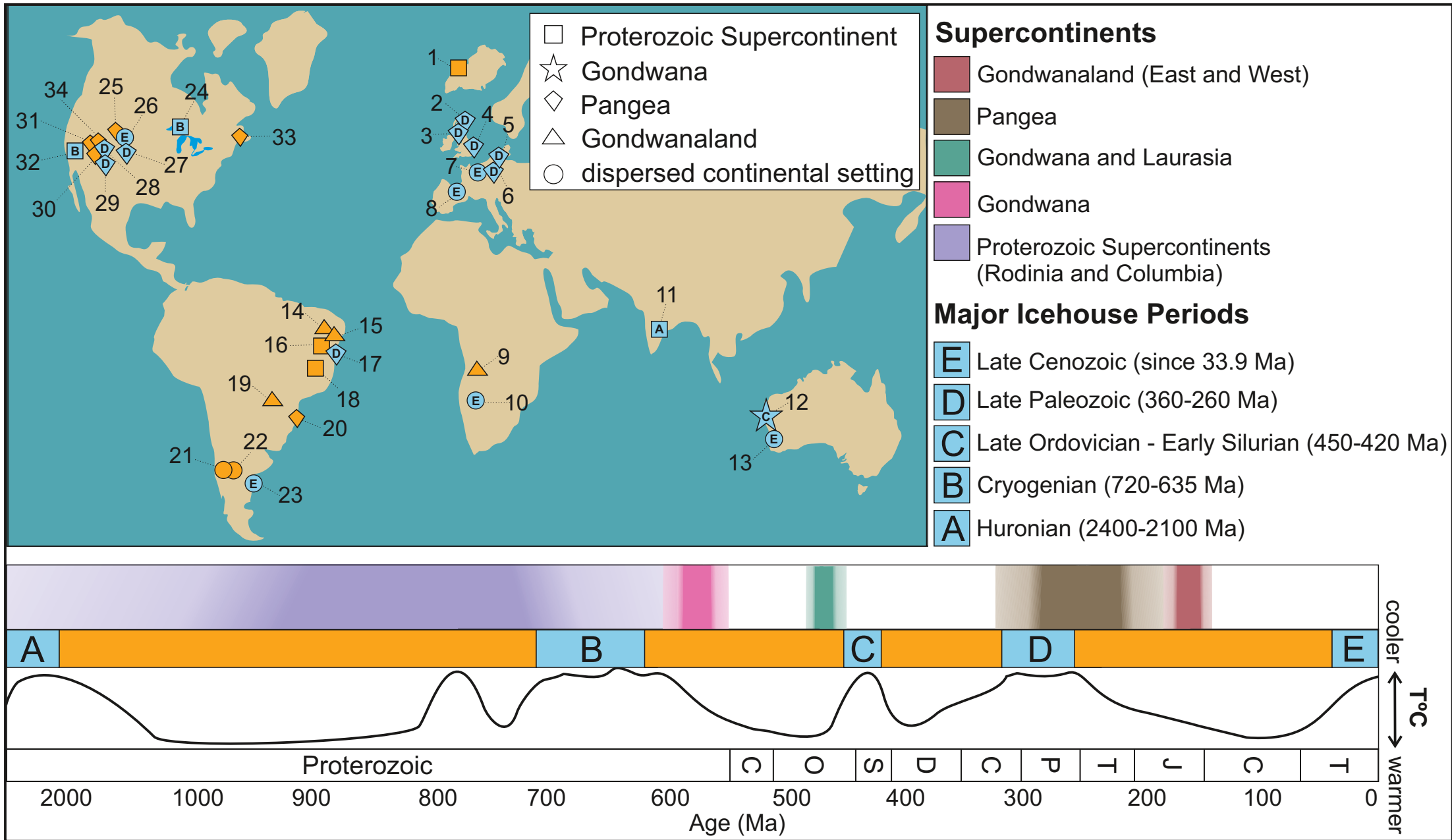
Figure 2
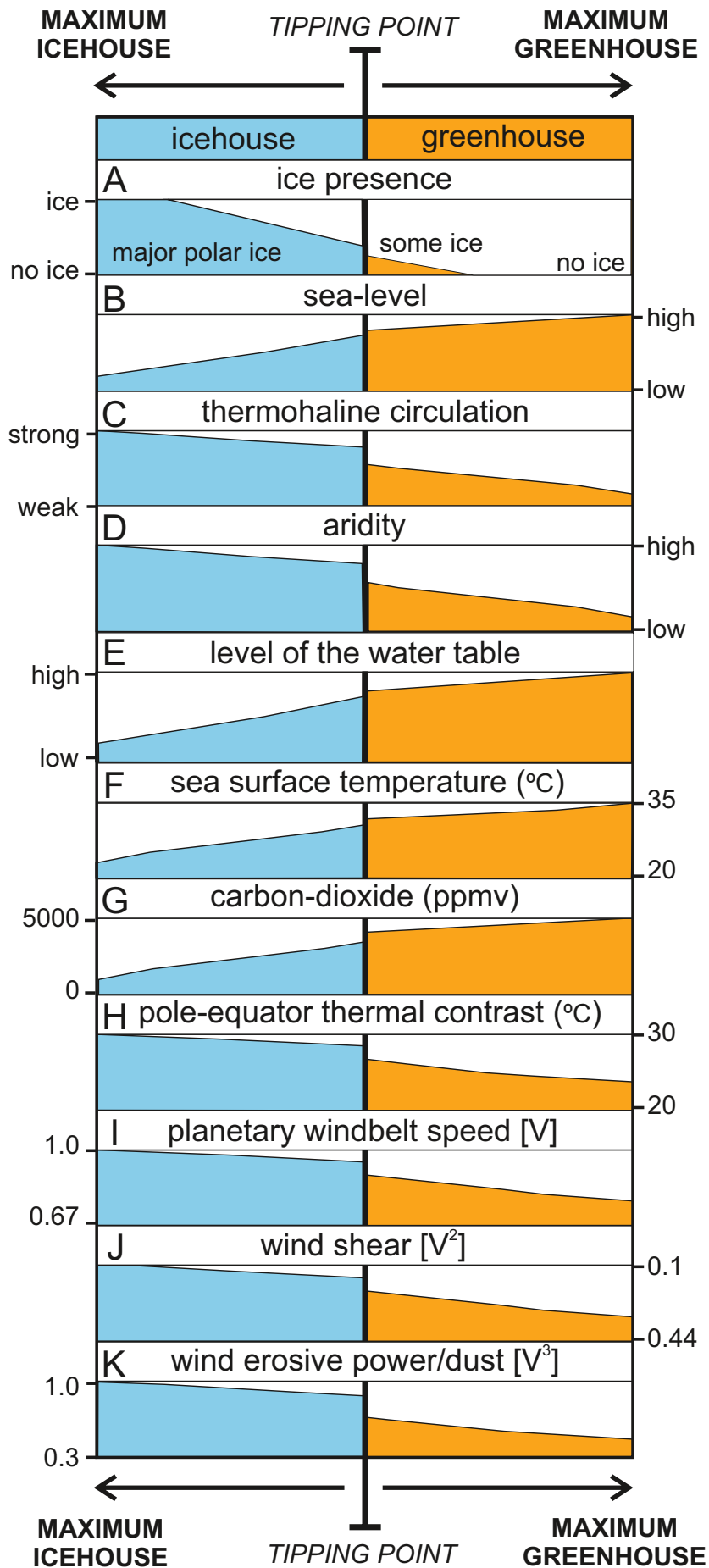
Figure 3
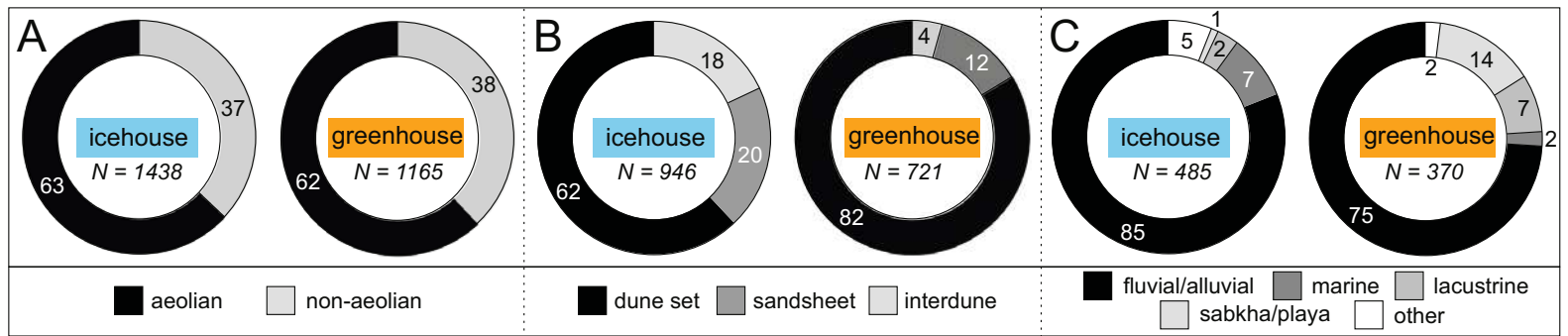
Figure 4
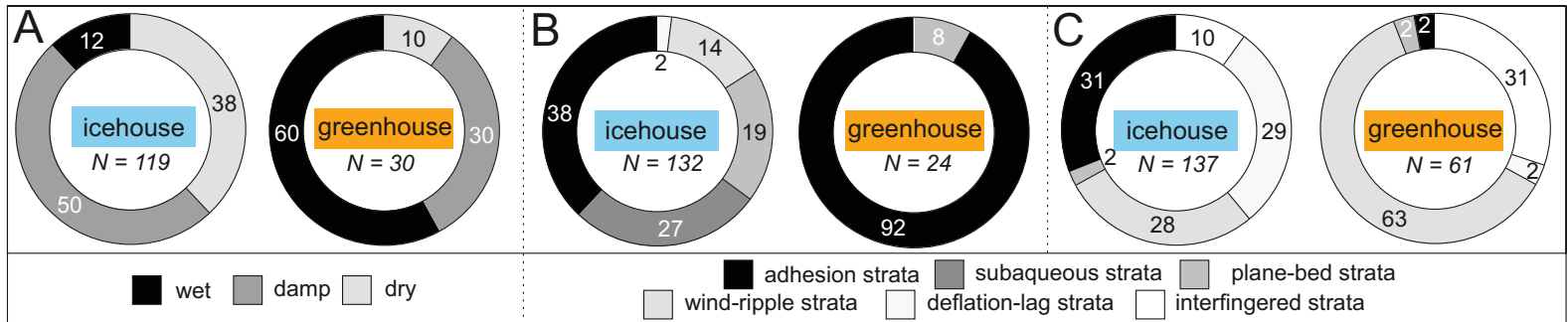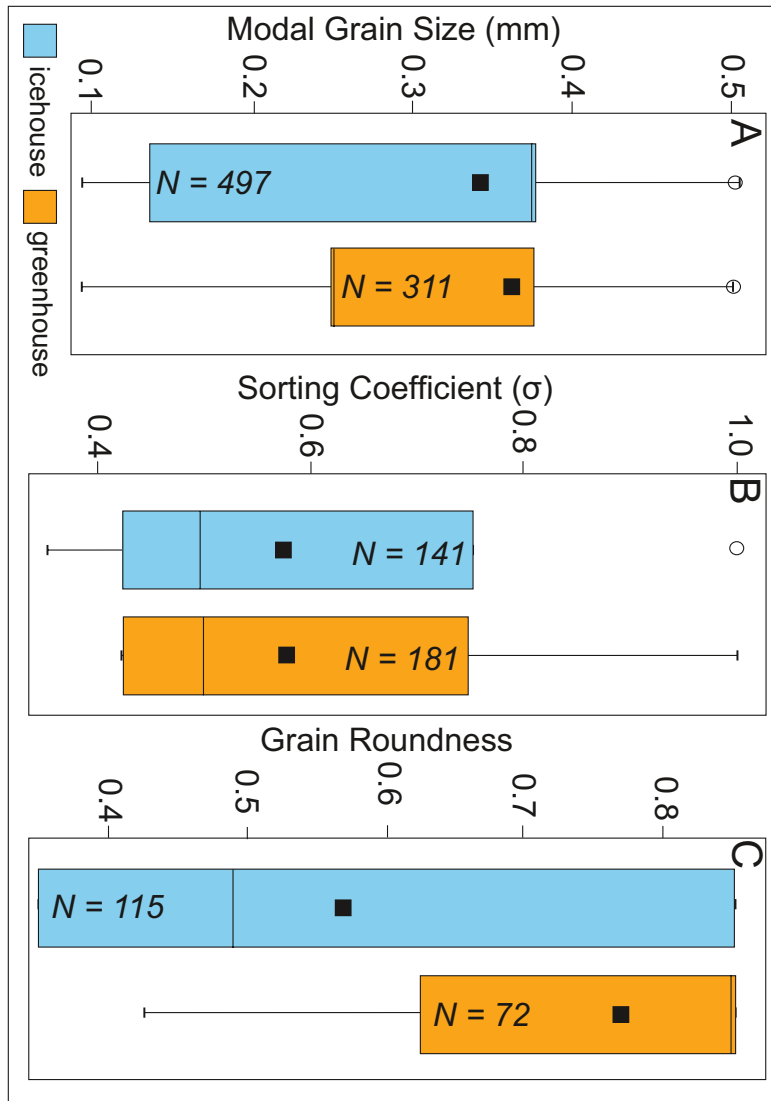
Figure 5
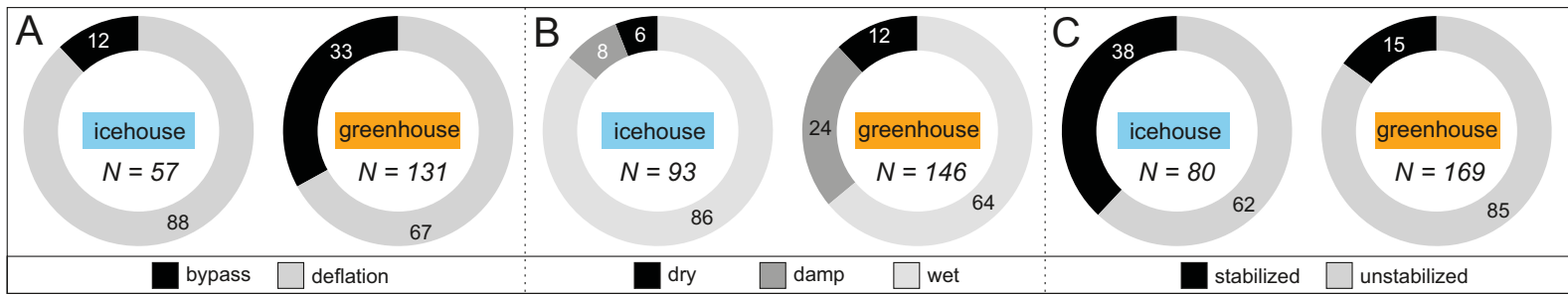
Figure 6

Figure 7

Figure 8
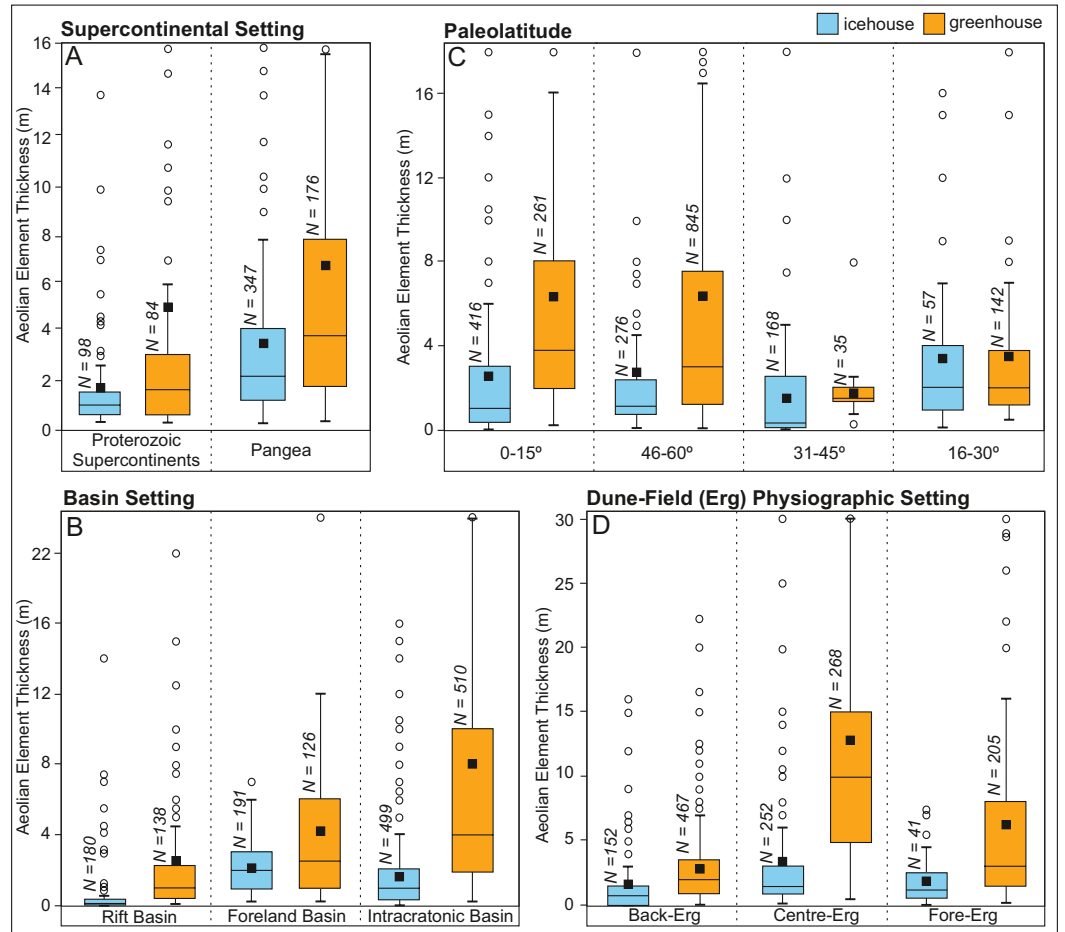
Figure 9

Figure 10

Figure 11

A

B

C

D

10s-100s m

10s m - km scale

SS

SS

SS

SS

accommodation   dune set   fluvial facies   SS-SS supersurface

underlying strata   sabkha   water table
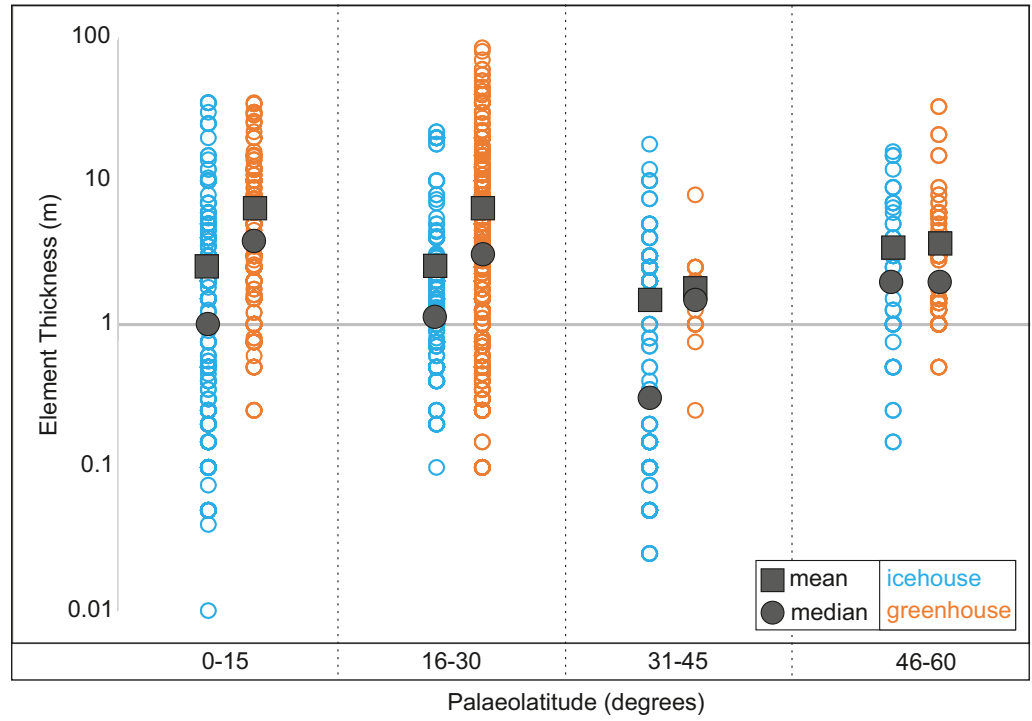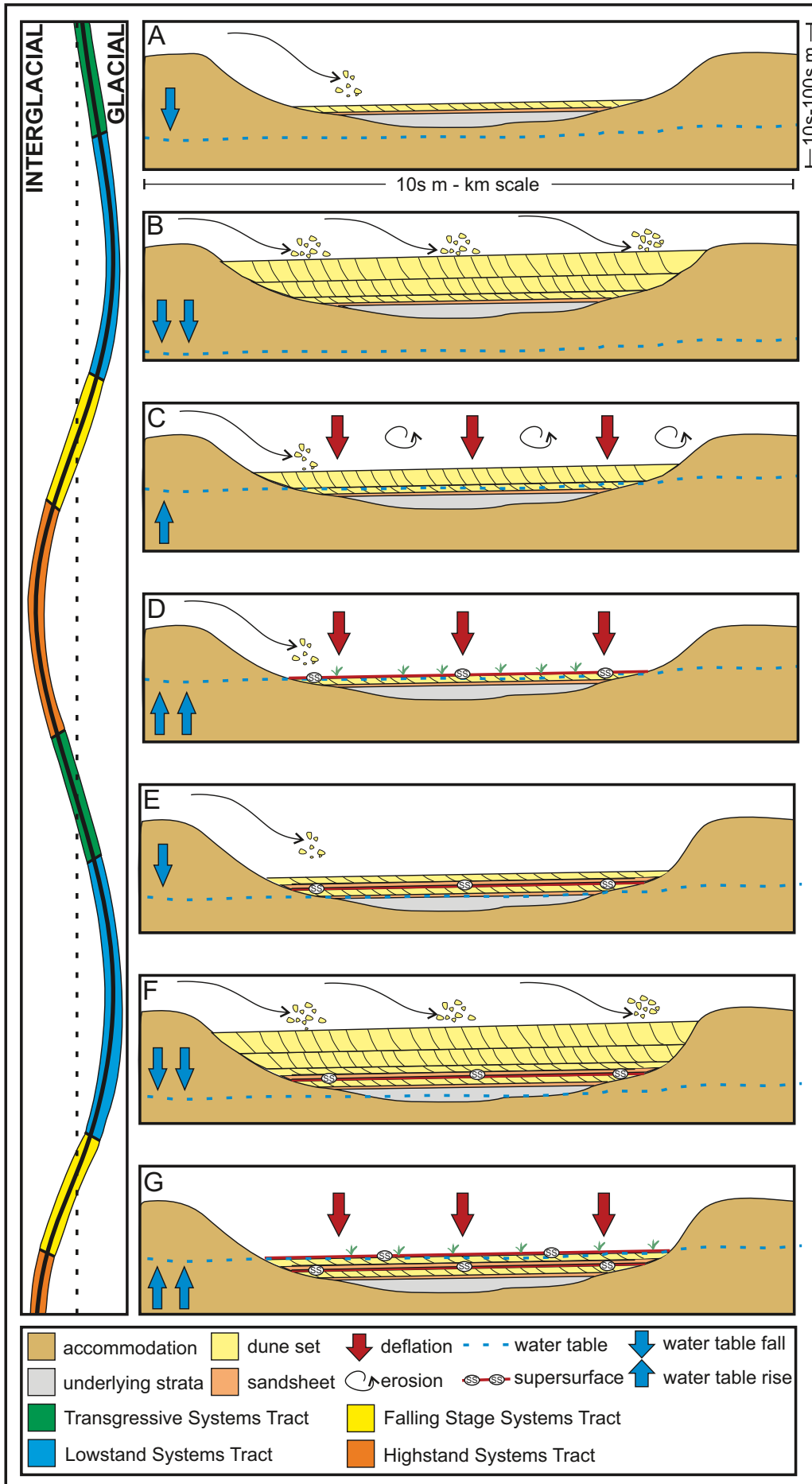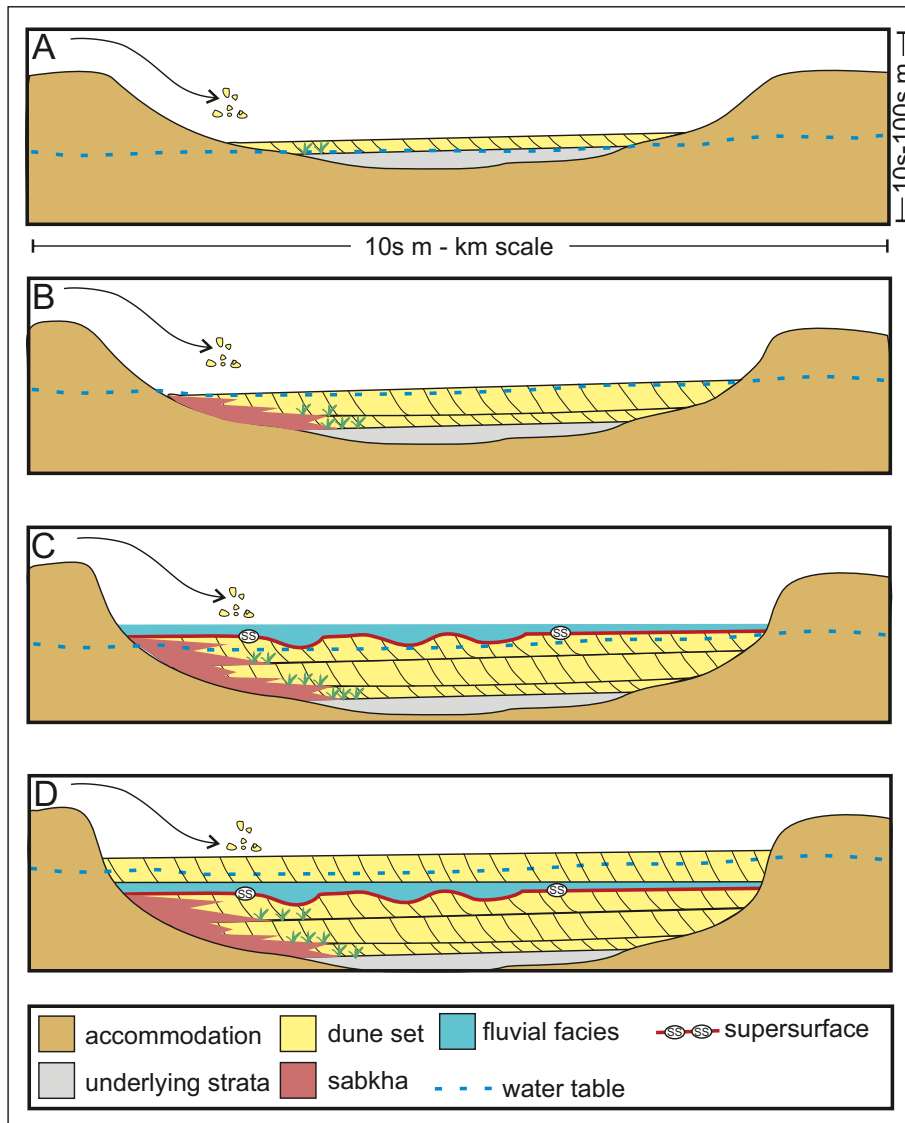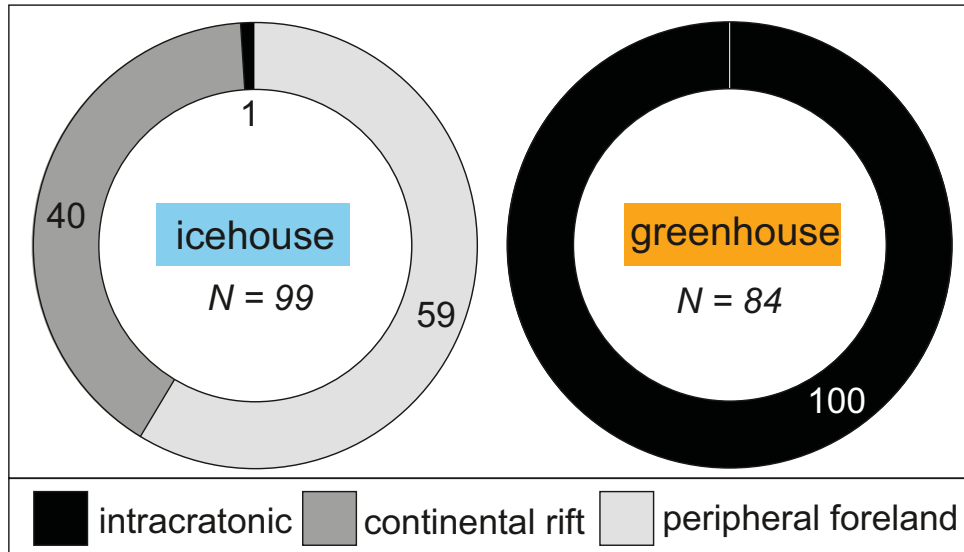
Figure 12

Figure 13
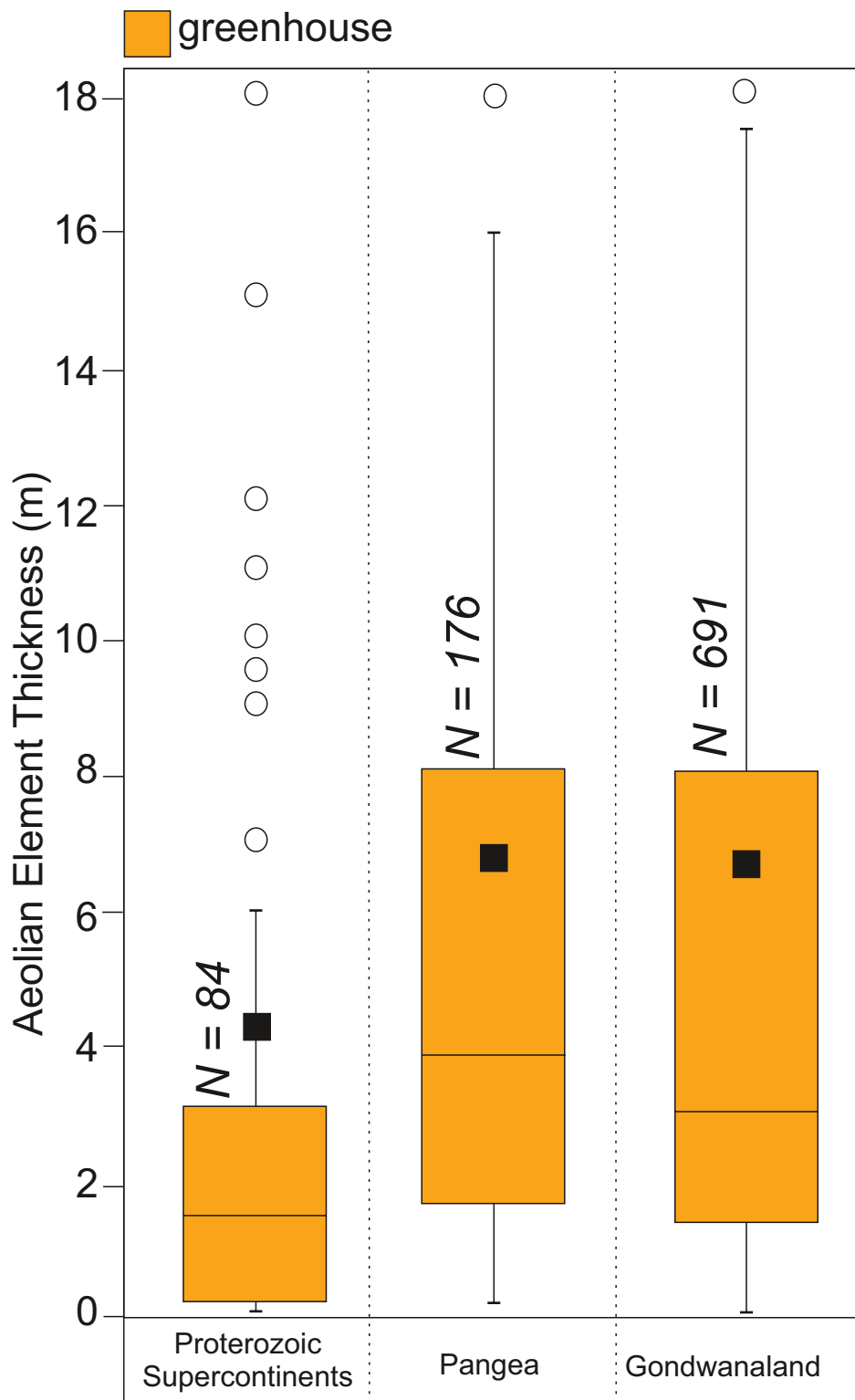
Table 1: Case study details					
Case Number	Icehouse or Greenhouse	Age (Ma)	Case Study Name	Location	Reference(s)
1	Greenhouse	ca. 1320 - 1000	Eriksfjord Formation	Greenland	Clemmenesen (1988)
2	Icehouse	ca. 259 - 254	Hopeman Sandstone	Scotland, UK	Clemmensen (1987)
3	Icehouse	ca. 290 - 240	Arran Red Beds	Isle of Arran, Scotland, UK	Clemmensen and Abrahamsen (1983)
4	Icehouse	ca. 252 - 242	Sherwood Sandstone	UK (Onshore and Offshore England and Northern Ireland)	Cowan (1993); Meadows and Beach (1993)
5	Icehouse	ca. 299 - 252	Rotliegendes Sandstone	Germany, Poland, Denmark, Baltic Sea, Netherlands	Ellis (1993); Newell (2001)
6	Icehouse	< 1	Boxtel Formation	Netherlands, Germany, Denmark, Poland	Schokker and Koster (2004)
7	Icehouse	ca. 38 - 34	Sable de Fontainbleau Formation	France	Cojan and Thiry (1992)
8	Icehouse	ca. 5	Escorihuela Formation	NE Spain	Liesa et al. (2016)
9	Greenhouse	ca. 132	Etjo Formation	Namibia	Mountney and Howell (2000)
10	Icehouse	ca. 23 - 3	Tsondab Sandstone	Namibia	Kocurek et al. (1999)
11	Icehouse	ca. 2500 - 2250	Egalapenta Formation	India	Biswas (2005); Dasgupta et al. (2005)
12	Icehouse	ca. 430 - 420	Tumblagooda Formation	Australia	Trewin (1993)
13	Icehouse	ca. 3	Tamala Limestone	Australia	Semeniuk and Glassford (1988)
14	Greenhouse	ca. 140 - 125	Sao Sebastio Formation	Brazil	Formola Ferronatto et al. (2019)
15	Greenhouse	ca. 148 - 144	Sergi Formation	Brazil	Scherer et al. (2007)
16	Greenhouse	ca. 1800 - 1600	Mangabeira Formation	Brazil	Ballico et al. (2017)
17	Icehouse	ca. 298 - 272	Caldeirao Formation	Brazil	Jones et al. (2015)
18	Greenhouse	ca. 1800 - 1700	Bandeirinha Formation	Brazil	Simplicio and Basilici (2015)
19	Greenhouse	ca. 163 - 145	Guara Formation	Brazil	Scherer and Lavina (2005)
20	Icehouse	ca. 260	Piramboia Formation	Brazil	Dias and Scherer (2008)
21	Greenhouse	ca. 129 - 125	Huitrin Formation	Argentina	Strömbäck et al. (2005)
22	Greenhouse	ca. 130 - 129	Agrio Formation	Argentina	Veiga et al. (2002)
23	Icehouse	ca. 10 - 4	Rio Negro Formation	Argentina	Zavala and Frieje (2001)
24	Icehouse	ca. 720 - 640	Copper Habor	Michigan, USA	Taylor and Middleton

			Formation		(1990)
25	Greenhouse	ca. 250 - 245	Chugwater Formation	Wyoming, USA	Irmen and Vondra (2000)
26	Icehouse	ca. 23 - 16	Arikaree Formation	Wyoming, Nebraska, USA	Bart (1977)
27	Icehouse	ca. 299 - 280	Ingleside Formation	Colorado, Wyoming, USA	Pike and Sweet (2018)
28	Icehouse	ca. 299- 280	Lower Cutler Beds	Utah, USA	Jordan and Mountney (2010)
29	Icehouse	ca. 286 - 245	Cedar Mesa Sandstone	Utah, Colorado, New Mexico, Arizona, USA	Loope (1985); Mountney and Jagger (2004); Mountney (2006)
30	Greenhouse	ca. 201 - 191	Navajo Sandstone	Nevada, Arizona, Colorado, Utah, USA	Loope and Rowe (2003)
31	Greenhouse	ca. 166 - 163	Entrada Sandstone	Wyoming, Utah, Arizona, New Mexico, Texas, USA	Crabaugh and Kocurek (1993); Benan and Kocurek (2000); Kocurek and Day (2018)
32	Icehouse	ca. 2500 - 2250	Big Bear Formation	California, USA	Stewart (2005)
33	Greenhouse	ca. 227 - 210	Wolfville Formation	Nova Scotia, Canada	Leleu and Hartley (2018)
34	Greenhouse	ca. 170 - 166	Page Sandstone	Arizona, Utah, Wyoming, USA	Jones and Blakey (1997); Kocurek et al. (1992)

Table 1: List of the case studies used in this investigation. The geographic location of each case study is outlined in Figure 1 (identified via the case number). The reference refers to the original source material from which quantitative metrics were derived.

Table 2: List of definitions used in the text	
Eolian Architectural Element Types	
Cross-strata package	Packages of aeolian stratification (typically composed of wind-ripple, grainflow and grainfall strata; Hunter 1977, 1981); form parts of dune sets; packages of cross-strata are typically separated by reactivation surfaces (Brookfield, 1977; Kocurek, 1996).
Dune set	Dune-sets form the fundamental unit of deposition of an eolian sand dune; dune-sets are formed of packages of cross-strata (Sorby, 1859; Allen, 1963; Rubin and Hunter 1982; Chrintz and Clemmensen, 1993); if dune sets migrate over each other, cross-stratified packages are truncated, delineating sets that are bounded by erosional surfaces (Brookfield, 1977; Kocurek, 1996).
Dune coset	Two or more genetically related dune sets that occur in vertical succession; both the coset and its contained sets are separated by bounding surfaces (Brookfield, 1977; Kocurek, 1996).
Dune compound set	A specialized class of coset wherein the contained sets record the migration of formative bed forms of a common type, for example where dunes migrate over the flanks of a parent megabedform (draa) which is itself migrating to leave an accumulation; both the compound set and its contained sets are separated by bounding surfaces (Brookfield, 1977; Kocurek, 1996).
Sandsheet	Sandsheet deposits are low-relief accumulations of eolian sediment in areas where dunes are generally absent (Nielsen and Kocurek, 1986; Brookfield, 1992; Rodríguez-López et al., 2012); sandsheets can also comprise low-relief bedforms such as zibars.
Interdune	Interdune deposits are formed in the low-relief, flat, or gently sloping areas between dunes; neighboring dunes are separated by interdunes (Hummel and Kocurek, 1984).
Dry interdune	Dry interdunes are characterized by deposits that accumulate on a substrate where the water table is well below the ground surface, such that sedimentation is not controlled by and is largely not influenced by the effects of moisture (Fryberger et al., 1990).
Damp interdune	Damp interdunes are characterized by deposits that accumulate on a substrate where the water table is close to the ground surface, such that sedimentation is influenced by the presence of moisture (Fryberger et al., 1988; Lancaster and Teller, 1988; Kocurek et al., 1992).
Wet interdune	Wet interdunes are characterized by deposits that accumulate on a substrate where the water table is elevated above the ground surface such that the interdune is episodically or continuously flooded with water (Kocurek and Havholm, 1993; Loope et al., 1995; García-Hidalgo et al., 2002).
Eolian Facies Element Types	
Wind-ripple strata	Wind-ripple lamination forms when wind-blown, saltating grains strike sand-grains obliquely and propel other grains forward (Bagnold, 1941; Hunter, 1977). The foreset laminae of wind-ripple strata are occasionally preserved (rippleform laminae), however, the internal laminae of wind-ripple strata are often indistinguishable due to grain size uniformity (translatent wind-ripple stratification; Hunter, 1977).
Grainflow strata	Grainflow strata form where a dune slipface undergoes gravitational collapse (Hunter, 1977; Bristow and Mountney, 2013). Grainflow deposits are typically erosionally based and are devoid of internal structure, forming discrete tongues or wide sheets of inclined strata on the lee-slope of dunes, which wedge-out towards the base of the dune. Individual grainflow strata may be indistinguishable, resulting in amalgamated grainflow units (Howell and Mountney, 2001).
Grainfall strata	Grainfall strata are gravity-driven deposits that occur when the wind transports saltating clouds of grains beyond a dune brink; grains settle onto the upper portions of lee slopes as wind transport capacities reduce in the lee-side depressions (Nickling et al., 2002). Grainfall laminae are typically thin (<1 mm), drape existing topography, else may have a wedge-shaped geometry; grainfall lamination is generally composed of sand and silt or (rarely) clay sizes grains (Hunter, 1977).

Interfingered strata	Interfingered strata represent intercalated packages of wind-ripple, grainflow, grainfall and plane-bed strata; two or more of the aforementioned stratal types may be present. This composite facies type is used only in cases where it is not possible to differentiate individual wind-ripple, grainflow, grainfall or plane-bed facies elements. Interfingered strata can occur in a variety of eolian settings and are especially common on dune lee slopes (Hunter, 1977; Hunter, 1981).
Adhesion strata	Adhesion strata results from the adhesion of moving grains to a damp surface, such as a damp interdune (Hummel and Kocurek, 1984). Adhesion strata typically are low relief (several mm in height) and exhibit sub-horizontal structures with irregular surfaces. Adhesion strata can comprise adhesion plane beds, adhesion ripples (Kocurek and Fielder, 1982) and adhesion warts (Olsen et al., 1989).
Plane-bed strata	Plane-bed lamination forms when wind velocities are too high to form ripples (Hunter 1977, 1981). Plane-bed lamination is composed of (sub)horizontally laminated sand, which typically dips at angles of between 0 and 15° (Pye, 2009). Plane-bed laminae are typically millimeter-scale, with sharp or gradational contacts (e.g., Clemmensen and Abrahamsen, 1983) and form sets typically up to 100 mm (Pye, 2009).
Subaqueous ripple strata	Subaqueous ripple lamination is generated by tractional processes and are produced by the action of waves or currents on a sediment surface (Allen, 1978).
Non-Eolian Element Types	
Fluvial/Alluvial	Deposits arising from or relating to the action of rivers/streams and sediment gravity-flow processes (cf. Melton, 1965).
Marine	Deposits arising from or relating to accumulation in marine environments.
Lacustrine	Deposits arising from or relating to accumulation in perennial lakes.
Sabkha/Playa	Sabkhas and playa lakes describe low-relief flats where evaporites, and in some cases carbonates, accumulate. The terms sabkha and playa lake were originally used to describe coastal and inland settings, respectively (Evans, et al., 1964; Purser and Evans, 1973); however, the terms are now commonly used interchangeably.
Other	Any depositional element that differs in origin from those above.
Surface Types	
Supersurface	Surfaces resulting from the cessation of eolian accumulation; occurs where the sediment budget switches from positive to negative (cannibalization of eolian system) or neutral (zero angle of climb), resulting in deflation (*deflationary supersurface*) or bypass (*bypass supersurface*) of the eolian system, respectively. Supersurfaces are also generated by changes in depositional environment, such as transition from eolian to fluvial, or eolian to marine deposition (e.g., Glennie and Buller, 1983; Chan and Kocurek, 1988).
Wet-type supersurface	Supersurface associated with deflation down to the water-table (also known as a Stokes surface). Wet-type supersurfaces may be associated with aqueous inundation by a non-eolian source (e.g., fluvial/marine deposits).
Damp-type supersurface	Supersurface associated with bypass/deflation; the level of the water table is interacting with the surface.
Dry-type supersurface	Supersurface associated with bypass/deflation; the level of the water table is significantly below the surface.
Basin Types	
Intracratonic (sag) basins	An intracratonic (sag) basin is a depressed or persistently low area occurring in the interior of cratonic blocks or on stable continental crust (Middleton, 1989); they are characterized by generally low rates of accommodation generation, and host sedimentary infills that can be >10 km in thickness and that typically embody over 200-800 Myr (Einsele, 2013).
Rift basin	A continental rift is an elongate graben or half-graben trough (ca. 10^3-10^4 km^2) bounded by normal faults, associated with active lithospheric extension and thinning (Gregory, 1894); rift basins are characterized by high rates of accommodation generation (e.g., Rosendahl, 1987; Schlische, 1993; Morley, 1995; Withjack et al., 2002).
Foreland basins	A foreland basin is here defined as a depression generated by flexure of the continental crust in front of a fold-and-thrust mountain belt (Einsele, 2013) and are characterized by intermediate rates of accommodation generation.

Table 2: Definitions of eolian and non-eolian architectural elements, facies elements, surface types, and basin types discussed in the text.

Table 3: Results of statistical analyses					
ARCHITECTURAL AND FACIES ELEMENT THICKNESS					
	EOLIAN ARCH. EL.		*NON-EOLIAN ARCH. EL.*		*FACIES ELEMENTS*	
	ICEHOUSE	GREENHOUSE	ICEHOUSE	GREENHOUSE	ICEHOUSE	GREENHOUSE
MEAN	2.36	5.47	5.18	4.88	2.20	7.53
MEDIAN	1.00	2.50	2.00	2.00	1.00	3.75
SD	4.48	8.40	10.07	12.24	3.93	10.23
N	789	903	367	519	630	355
P(T<=t)	0.00		0.35		0.00	
SIGNIFICANT?	TRUE		FALSE		TRUE	
SPECIFIC EOLIAN ELEMENTS					
	DUNE SET		*SANDSHEET*		*INTERDUNE*	
	ICEHOUSE	GREENHOUSE	ICEHOUSE	GREENHOUSE	ICEHOUSE	GREENHOUSE
MEAN	3.67	5.93	0.55	4.15	0.88	2.00
MEDIAN	2.00	3.00	0.20	2.00	0.25	1.50
SD	5.54	7.94	0.88	10.33	1.74	2.75
N	440	705	183	171	166	27
P(T<=t)	0.00		0.00		0.00	
SIGNIFICANT?	TRUE		TRUE		TRUE	
EOLIAN TEXTURE					
	GRAIN SIZE		*SORTING*		*ROUNDNESS*	
	ICEHOUSE	GREENHOUSE	ICEHOUSE	GREENHOUSE	ICEHOUSE	GREENHOUSE
MEAN	0.34	0.36	0.57	0.58	0.57	0.77
MEDIAN	0.38	0.25	0.50	0.50	0.49	0.85
SD	0.27	0.25	0.19	0.19	0.22	0.12
N	496	310	140	179	113	70
P(T<=t)	0.14		0.43		0.00	
SIGNIFICANT?	FALSE		FALSE		TRUE	
EOLIAN ARCHITECTURAL ELEMENTS BY SUPERCONTINENTAL SETTING					
	PROTEROZOIC SUPERCONTINENTS			*PANGEA*		
	ICEHOUSE		GREENHOUSE	ICEHOUSE		GREENHOUSE
MEAN	1.43		5.04	3.41		6.85
MEDIAN	0.80		1.50	2.00		3.86
SD	2.41		14.44	5.31		7.87
N	98		84	347		176
P(T<=t)	0.02			0.00		

SIGNIFICANT?	TRUE			TRUE		

EOLIAN ARCHITECTURAL ELEMENTS BY BASIN SETTING

	INTRACRATONIC BASIN		*CONTINENTAL RIFT BASIN*		*FORELAND BASIN*	
	ICEHOUSE	GREENHOUSE	ICEHOUSE	GREENHOUSE	ICEHOUSE	GREENHOUSE
MEAN	1.73	7.63	0.70	2.48	2.11	4.23
MEDIAN	1.00	3.50	0.15	1.00	2.00	2.50
SD	2.24	10.77	2.00	3.69	1.44	4.47
N	507	595	138	180	191	126
P(T<=t)	0.00		0.00		0.00	
SIGNIFICANT?	TRUE		TRUE		TRUE	

EOLIAN ARCHITECTURAL ELEMENTS BY PALAEOLATITUDE

	0-15 DEGREES		*16-30 DEGREES*	
	ICEHOUSE	GREENHOUSE	ICEHOUSE	GREENHOUSE
MEAN	2.60	6.38	2.72	6.40
MEDIAN	1.00	3.75	1.10	3.00
SD	4.84	7.08	4.57	9.82
N	416	261	276	845
P(T<=t)	0.00		0.00	
SIGNIFICANT?	TRUE		TRUE	

	31-45 DEGREES		*46-60 DEGREES*	
	ICEHOUSE	GREENHOUSE	ICEHOUSE	GREENHOUSE
MEAN	1.53	1.75	3.39	3.50
MEDIAN	0.30	1.50	2.00	2.00
SD	2.42	1.21	3.92	4.76
N	168	35	57	142
P(T<=t)	0.30		0.44	
SIGNIFICANT?	FALSE		FALSE	

EOLIAN ARCHITECTURAL ELEMENTS BY ERG DISTALITY

	BACK ERG		*CENTER ERG*		*FORE ERG*	
	ICEHOUSE	GREENHOUSE	ICEHOUSE	GREENHOUSE	ICEHOUSE	GREENHOUSE
MEAN	1.65	2.92	3.39	12.83	1.87	6.36
MEDIAN	0.75	2.00	1.50	10.00	1.20	3.00
SD	2.79	3.22	5.96	11.75	1.81	7.37
N	152	467	252	268	41	205

P(T<=t)	0.00		0.00	0.00
SIGNIFICANT?	TRUE		TRUE	TRUE

COMPARISONS OF GREENHOUSE PANGEAN DEPOSITS WITH OTHER GREENHOUSE SUPERCONTINENTAL SETTINGS

	GREENHOUSE ONLY		GREENHOUSE ONLY	
	PANGEA	*GONDWANALAND*	*PANGEA*	*PROTEROZOIC SUP.*
MEAN	6.85	6.70	6.85	4.26
MEDIAN	3.88	3.00	3.88	1.50
SD	7.87	9.43	7.87	12.63
OBSERVATIONS	176	691	176	84
ANOVA	0.85		0.04	
SIGNIFICANT?	FALSE		FALSE	

SUPERSURFACE SPACING

	ICEHOUSE	GREENHOUSE
MEAN	16.34	9.07
MEDIAN	16.00	9.00
SD	12.70	6.34
OBSERVATIONS	25	7

Table 3: Results of statistical analyses; SD: standard deviation; P(T<=t): one tail t-test; ANOVA: analysis of variance. All results are reported to two decimal places, where appropriate. For all statistical calculations see Supplementary Information.